

Experimental Study of Extinguishing Shielded Fires by a Low-pressure Multi-orifice Water Mist Nozzle

Original

Experimental Study of Extinguishing Shielded Fires by a Low-pressure Multi-orifice Water Mist Nozzle / Hamzehpour, A., Verda, V., Borchiellini, R.. - In: FIRE SAFETY JOURNAL. - ISSN 0379-7112. - (2024). [10.1016/j.firesaf.2024.104175]

Availability:

This version is available at: 11583/2988356 since: 2024-05-09T12:51:19Z

Publisher:

Elsevier

Published

DOI:10.1016/j.firesaf.2024.104175

Terms of use:

This article is made available under terms and conditions as specified in the corresponding bibliographic description in the repository

Publisher copyright

(Article begins on next page)



Experimental study of extinguishing shielded fires by a low-pressure multi-orifice water mist nozzle

Azad Hamzehpour^{*}, Vittorio Verda, Romano Borchiellini

Department of Energy (DENEG), Politecnico di Torino, Corso Duca degli Abruzzi 24, 10129, Turin, Italy

ARTICLE INFO

Keywords:

Fire safety
Water mist system
Shielded fire
Fire suppression
PDPA

ABSTRACT

The performance of a water mist system to suppress shielded fires is analyzed experimentally in this work. The diesel pool fire is used as the fire source in an enclosure with 2.4 m × 2.4 m × 3.1 m measurements, and a mechanism is designed to provide different shielding conditions by changing the obstacle size and height. The characteristics of a low-pressure multi-orifice nozzle including the drop diameter and the velocity are studied by a Phase Doppler Particle Analyzer (PDPA) system. In total, 10 cases with diverse shielding conditions are defined and different parameters including the temperature distribution, the gas concentrations, and the extinguishing time are measured. Based on the present data, mist droplets in some shielded fire scenarios were able to bypass the obstacle, overcome the fire plume thrust, and suppress the fire. In fire scenarios with the same obstruction size, the reduction of the distance between the obstacle and the nozzle led to an increased block ratio and consequently, the extinguishing time was decreased. It was found that the temperatures in the central axis above the fire and the lateral temperatures declined quickly in cases with short suppression time.

Nomenclature

$D_{V0.5}$	droplet diameter such that 50 % of the total liquid volume is in droplets of smaller diameters (μm)
$D_{V0.9}$	droplet diameter such that 90 % of the total liquid volume is in droplets of smaller diameters (μm)
$D_{V0.99}$	droplet diameter such that 99 % of the total liquid volume is in droplets of smaller diameters (μm)
F_f	Fire plume momentum at nozzle location (kg.m/s)
F_w	Initial spray momentum (kg.m/s)
H	Vertical distance between the obstacle and the floor (cm)
h	Vertical distance between the spray and the fuel pan upper surface (m)
h_s	Vertical distance between the spray and the obstacle (m)
ΔH_c	Heat of combustion (kJ.kg^{-1})
k	Flow coefficient ($\text{l/min/bar}^{1/2}$)
k_p	Block ratio
L	Height of flame (m)
L_0	Length of the obstacle (m)
L_f	Length of the fuel pan (m)
L_p	Projection length of the mist spray to the fuel surface formed by the obstacle (m)
\dot{m}_{fuel}	Burning rate of the fuel (kg/s)
\dot{m}_p	Fire plume mass flux at nozzle location (kg/s)
\dot{m}^*	Mass loss rate per unit area ($\text{kg/m}^2\cdot\text{s}$)
p	Working pressure (bar)

(continued on next column)

(continued)

Q	Water flow rate (l/min)
\dot{Q}	HRR (kW)
\dot{Q}_c	Convective part of HRR (kW)
T_0	Ambient temperature ($^{\circ}\text{C}$)
u_0	Upward plume velocity at nozzle location (m/s)
U_0	Initial droplet velocity (m/s)
\dot{V}	Water discharge rate (kg/s)
z	Height of fire plume (m)
z_0	Height of virtual origin of fire plume (m)
Greek symbols	
α	Plume-spray thrust ratio
θ_0	Geometric angle formed by the mist spray and the obstacle ($^{\circ}$)
\varnothing	Combustion efficiency
Abbreviations	
CFD	Computational Fluid Dynamics
FDS	Fire Dynamics Simulator
HRR	Heat release rate
MLR	Mass Loss Rate
PDIA	Particle/Droplet Image Analyzer
PIV	Particle Image Velocimetry
PDPA	Phase Doppler Particle Analyzer
PMT	Photomultiplier Tube
SMD	Sauter Mean Diameter
TC	Thermocouple
VMD	Volumetric Median Diameter

^{*} Corresponding author.

E-mail address: azad.hamzehpour@polito.it (A. Hamzehpour).

<https://doi.org/10.1016/j.firesaf.2024.104175>

Received 27 December 2023; Received in revised form 8 April 2024; Accepted 6 May 2024

Available online 7 May 2024

0379-7112/© 2024 The Authors. Published by Elsevier Ltd. This is an open access article under the CC BY license (<http://creativecommons.org/licenses/by/4.0/>).

1. Introduction

In recent decades, fire safety engineers and researchers have been trying to develop more reliable active fire suppression systems. Fixed water-based fire-extinguishing systems including water mist systems are recognized as effective, reliable, and environmentally friendly tools for extinguishing and controlling fires. Water mist systems can be classified as low-pressure (pressure ≤ 12.1 bar), intermediate-pressure (between 12.1 and 34.5 bar), and high-pressure (34.5 bar \leq pressure) systems [1]. The technology of spray nozzles has been advanced in recent years to optimize their extinguishing performance for specific applications. Water mist systems are widely used in a variety of spaces like commercial/residential buildings, machinery spaces, and tunnels; however, using these systems for other fire risk applications like fire in electric cars is still challenging [2].

Numerous large-scale and reduced-scale fire tests in a variety of spaces were conducted to investigate the fire behavior while using water mist systems. These research works were mostly focused on the performance of suppression systems in extinguishing different types of fire. The effectiveness of water mist systems is usually evaluated with respect to the extinguishing time and the water consumption. In several studies, it was shown that water mist systems succeed in suppressing different types of fire, and dominant fire extinguishing mechanisms were discussed [3–5]. The application time of the water mist nozzle is of importance while investigating fire suppression tests. Jenft et al. [4] demonstrated that depending on the application time (early or late application), the dominant extinguishing mechanisms can be diverse.

Furthermore, the suppression performance is sensitive to the nozzle characteristics and can be improved by optimizing the spray flow rate and the cone angle [6], and this performance is also dependent on the fire size and type in an enclosure [7]. The mist droplet size can be altered by the working pressure of the nozzle and therefore the suppression performance and extinguishing mechanisms are affected [8,9]. The importance of ventilation conditions on water mist effectiveness in a compartment was pointed out by Zhou et al. [10], and it was seen that the extinguishing time with water mist nozzles is shorter in the presence of a mechanical ventilation system. However, the impact of ventilation conditions on the efficiency of water mist systems is more significant in tunnel fire scenarios and is thoroughly discussed in the literature [11–13]. Moreover, the location of the fire source from the spray nozzle is another factor influencing the efficiency of the suppression system [14]. It was shown that the closer the fire source to the mist nozzle, the shorter the extinguishing time. Due to the difficulties and high cost of performing experimental fire tests, Computational Fluid Dynamics (CFD) methods like Fire Dynamics Simulator (FDS) have become popular tools among fire safety scientists to investigate the performance of water-based fire suppression systems. The FDS can also be used to predict the optimum droplet size of water mist systems [15], to assess the effect of droplet size on the suppression performance [16,17], or to analyze the capability of FDS in determining water mist characteristics [18].

The above-mentioned nozzle characteristics can be measured experimentally by a variety of laser-based techniques developed to investigate the water discharge velocity and the diameter of the mist droplets in order to optimize the design of spray systems. The shadowgraph method is a simple and inexpensive way to measure the droplet size [19]. Wang et al. [20] employed the shadowgraph technique to measure the impact of ambient pressure on the water mist characteristics. A laser diffraction-based instrument like the Malvern-type droplet size analyzer was used to study the characteristics of a twin-fluid nozzle [21]. The same method was employed for measuring the droplet size of high-pressure nozzles [12,22]. The Particle/Droplet Image Analyzer (PDIA) assesses a specific volume occupied by drops and provides information about the droplet size temporally and spatially. Gupta et al.

[14] and Shrigondekar et al. [23] utilized this technology to characterize their water mist nozzles. Another tool for nozzle characterization is the Particle Image Velocimetry (PIV) method in which the displacement of imaged particles/droplets is measured to calculate the flow velocity through three stages including the image acquisition, the image interrogation, and the post-processing [24]. It is worth noting that employing this method for very small particles can be challenging [25]. Phase Doppler Particle Analyzer (PDPA) is another reliable tool for droplet size measurement and several research works utilized this technique [26,27].

For testing real fire scenarios, it is necessary to consider the existence of obstacles above the fire that can partially or completely block the access of mist drops to the flames or the fuel surface. These fire scenarios are called shielded fires and are likely to happen in many places like warehouses, storage units, or car and train fires in tunnels. There are a few studies focused on sheltered fire scenarios and the capability of water mist systems for such applications. Liu et al. [28] attempted to correlate the critical plume-spray thrust ratio and the block ratio in order to analyze the performance of water mist systems. This plume-spray thrust ratio was defined and formulated by Beihua et al. [29]. Alpert [30] explained the concept of the thrust of the flow induced by fires and the thrust of the spray droplets and the interaction between them. The shielded fire test in a tunnel with longitudinal ventilation was conducted by Liu et al. [13], and the impact of the obstacle above the fire on the temperature near the ceiling and the back-layering was demonstrated. In a sheltered fire scenario in a tunnel, it was shown that the fire suppression performance is dependent on the activation time [31]. The authors also reported that the main temperature control mechanism at low pressure of the water mist system is the dynamic effect. In a numerical study, it was seen that in some sheltered fire cases, the mist droplets can bypass the obstacle and penetrate the flame [32]. It was also proved that the suppression performance is sensitive to the obstacle size and its distance from the spray nozzle. Moreover, the extinguishing performance is also dependent on the relative position of the water mist system to the sheltered fire source, and the extinguishing time is larger in a shielded fire case compared to an unshielded one [33].

In realistic fire scenarios in different spaces like warehouses, tunnels, machinery spaces, and commercial areas, the fire source can be partially or completely covered by objects around. Relatively little is known about the shielded fire behavior and the capability of water mist systems for suppressing such fire scenarios. The effects of the obstruction size and the distance between the obstacle and the nozzle at the same time on the extinguishing performance are still unclear. In the present study, a series of experimental tests are conducted to comprehensively investigate the performance of water mist systems in suppressing shielded fires in a compartment with $2.4 \times 2.4 \times 3.1$ m³ measurements. Different shielding conditions including the obstruction size and its distance from the nozzle are considered to assess the suppression performance under these conditions. Two square pans with lengths of 25 cm and 30 cm are employed to provide the diesel pool fire with different Heat release Rates (HRRs). A multi-orifice spray nozzle with a working pressure of 10.5 bar is placed at the center axis of the enclosure above the fire and its characteristics are measured by a PDPA system. The temperature fields at various locations, the exhaust gas concentrations including O₂ and CO, and the extinguishing time for each case are among those parameters measured and reported in this work. The data presented in this paper is beneficial for better understanding the suppression process of more realistic fire scenarios in order to design and promote water mist systems for different applications.

2. Experimental procedure

2.1. Droplet size distribution and velocity

The characterization study of the spray system and the methodology for measuring the droplet size distribution are described in this section.

A PDPA system from TSI® with backscatter reflection configuration was set up, calibrated, and utilized to measure the characteristics of the low-pressure nozzle (K6 type, VID Fire-Kill) with one central and 6 peripheral orifices under no fire condition. The PDPA is a powerful method for velocity and diameter measurements. The comprehensive principles and explanations of the phase doppler and laser doppler measurement techniques can be found in Ref. [34]. The system components for the PDPA arrangement are listed in Table 1. The probes are installed on a 3D isel® traverse system to be moved to the specific coordinates.

After installation of the components, the output power is set to the proper value on the laser power controller. Then, the green laser beams on two couplers (shifted and unshifted) on the beam separator are aligned in a way that the intensity of the two beams on the couplers is evenly matched. The two beams emitted from the probe intersect at the measurement volume. A droplet crossing the intersection point scatters the light, and the scattered light is then captured and transmitted to the photomultiplier tubes (PMTs) through optical fibers. The signals are then processed for further analysis on the software. It is worth mentioning that PMTs and processing electronics may impact the phase shift measurements; therefore, a laser diode calibration is performed to eliminate these effects. The schematic diagram of the installed PDPA components is displayed in Fig. 1.

The measurements are obtained at a 5 cm vertical distance from the exit of the nozzle. The working pressure of the nozzle is set to 10.5 bar. When the measured valid counts reach the defined number, the capturing of data is stopped. The spray characteristics including the velocity and the diameter of mist droplets are obtained by FlowSizer™ software and will be represented and discussed in the results section.

2.2. Instrumentation and fire tests

The fire experiments are conducted in an enclosed space with $2.4 \times 2.4 \times 3.1 \text{ m}^3$ measurements, and a hood is placed above the compartment to collect the exhaust gas leading to a chimney using a mechanical fan. A $39.5 \times 39.5 \text{ cm}^2$ vent is designed in the lower part of the west side of the enclosure (the side with the glass door is the north side) to provide the make-up air. The precise location of the air vent is displayed in Fig. 2. Different diesel pool fire scenarios including dry and wet tests and shielded fire tests are performed separately. Two stainless steel square-shaped pans with the measurements of $25 \text{ cm} \times 25 \text{ cm}$ (pan 1) and $30 \text{ cm} \times 30 \text{ cm}$ (pan 2) with a height of 10 cm are employed for the pool fire tests, and the pool pan is placed in the middle of the compartment. The diesel is used as the fuel for all tests (approximately 200 g in pool pan 1 and 300 g in pool pan 2), and a small amount of ethanol with purity of 90 % (approximately 30 g) is added to the diesel for ignition purposes. For shielded fire tests, a mechanism (stainless steel) is constructed to provide different shielding conditions. This mechanism is adjustable in a way that different obstacle sizes can be placed at different heights above the pool fire. Three stainless steel obstacles with the measurements of $15 \text{ cm} \times 15 \text{ cm}$, $25 \text{ cm} \times 25 \text{ cm}$, and $40 \text{ cm} \times 40 \text{ cm}$ and the heights of 60 cm, 100 cm, and 160 cm above the floor are selected as variables to define different shielding conditions. A mass balance (PUE7.1.16HRP - Radwag®) protected by insulation layers is placed under the pan to measure the mass loss rate of the diesel during the dry fire test.

Table 1
Components of the PDPA system.

System component	Model
Laser	Coherent® Genesis™ MX series
Multicolor beam separator	Fiberlight
Transmitter/Transceiver probe	TM150
Photodetector module	PDM1000
Signal processor	FSA4000
Receiving probe	RV1100
Traverse system	3D isel® traverse system
FlowSizer™ software	FlowSizer 64 version 4.2.0

For the temperature measurement, three thermocouple trees with a total number of 30 thermocouples are designed and installed in the enclosure at different locations. One thermocouple tree is in the middle to measure the temperatures close to the fire, and 12 thermocouples are placed at different heights from 40 cm above the floor to 260 cm (M1-M12). The thermocouples in the middle are k-type (Chromel/Alumel), grounded with sheath material of Inconel 600, and the probe diameter of 1.6 mm (Tersid). Two other thermocouple trees are placed in the corners of the enclosure with 1 m offset from the central axis, and 9 thermocouples are installed on each tree at different heights, from 100 cm to 295 cm above the floor (C1,1-C1,9 and C2,1-C2,9). The characteristics of the thermocouples in the corners are the same as those in the middle except for the probe diameter which is 1 mm. One thermocouple is also installed outside the fire test room to record the ambient temperature. Two data loggers (Dletaohm) with a total number of 32 channels are used to collect the temperature data.

In order to measure the exhaust gas concentrations, a gas analyzer (Testo 330) is employed. The probe of the gas analyzer is inserted into the chimney and the oxygen and CO concentrations, and the temperature of the flue gas are measured every second during the experiment. An anemometer (Testo 405i) is placed at the vent to measure the inlet air flow rate. Moreover, a thermal camera (A6753sc-FLIR®) is installed outside the compartment to record the process of fire tests during each experiment. The measuring instruments used in this study and their accuracy are summarized in Table 2.

The low-pressure multi-orifice water mist nozzle (K6 type, VID Fire-Kill) is installed in the middle of the compartment at a height of 233 cm from the floor. A centrifugal vertical multistage electric pump (Caprari) connected to the piping system provides the water to the nozzle. A pressure gauge is used to control the working pressure, and an ultrasonic flowmeter (Portaflo PF330 - Micronics) is installed on the pipes to measure the water flow rate.

In total, 10 specific cases are defined as displayed in Table 3, and each specific test is conducted at least 3 times for repeatability purposes. The activation time of the water mist system for wet tests is at 150 s and 90 s after ignition when the pool length is 25 cm and 30 cm, respectively. Depending on the suppression time in each test, the water mist system is deactivated immediately after suppression; however, the maximum working time of the nozzle is 1 min. Each test lasts around 8 min, and the mechanical fan is always on during the test.

It should be noted that case 0 is a dry test with no use of water mist, and case 1 is a wet test with no shield. The schematic diagram of the fire test set-up along with the real photographs of the laboratory is depicted in Fig. 2. The detail of the vertical elevation level of thermocouples and their arrangements on each TC tree including one central tree and two lateral ones is displayed in Fig. 3.

3. Results and discussion

3.1. Spray characteristics

The characteristics of the water mist spray system used in this study for the fire suppression tests were obtained before the fire tests by a PDPA system. It is important to investigate the droplet size distribution as it can affect the performance of the fire extinguishing system. A wide range of droplet measurements can be obtained by the PDPA system including Sauter Mean Diameter (SMD or D_{32}), which is defined as the total volume of the droplet population divided by the total surface area of the droplet population, and the downward velocity. The mathematical representation of the droplet size distribution to characterize the experimental data can be defined by several functions such as Rosin-Rammler or log-normal distributions [35].

It should be noted that several characterization tests were conducted to analyze the effect of the set-up parameters on the velocity and drop size values and to find the optimum parameters. These parameters include PMT voltage, the output power, the burst threshold, the band

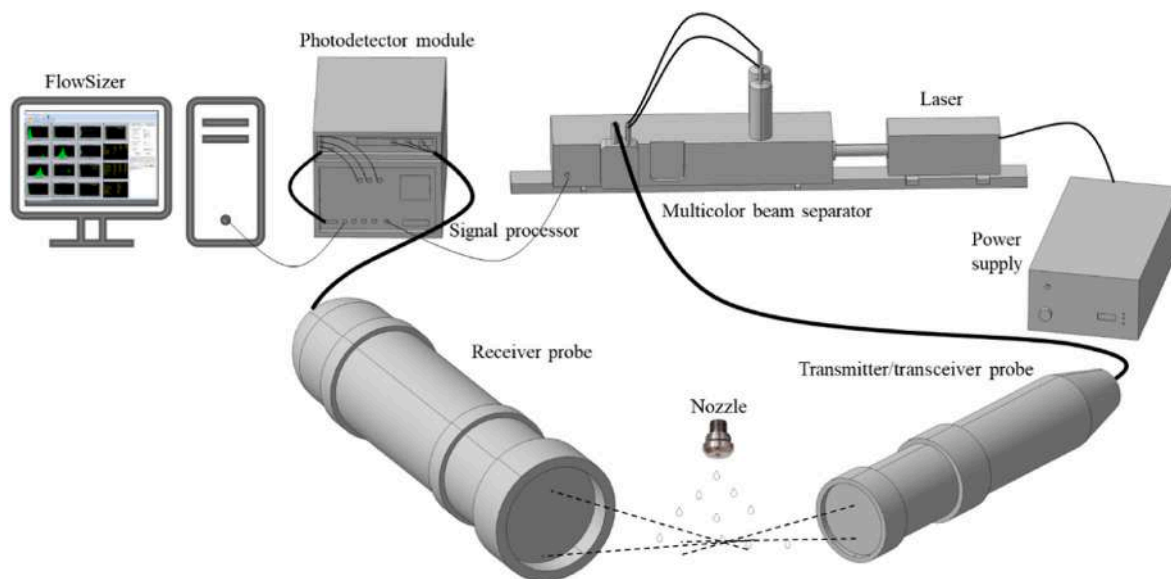


Fig. 1. Schematic view of the PDPA set-up.

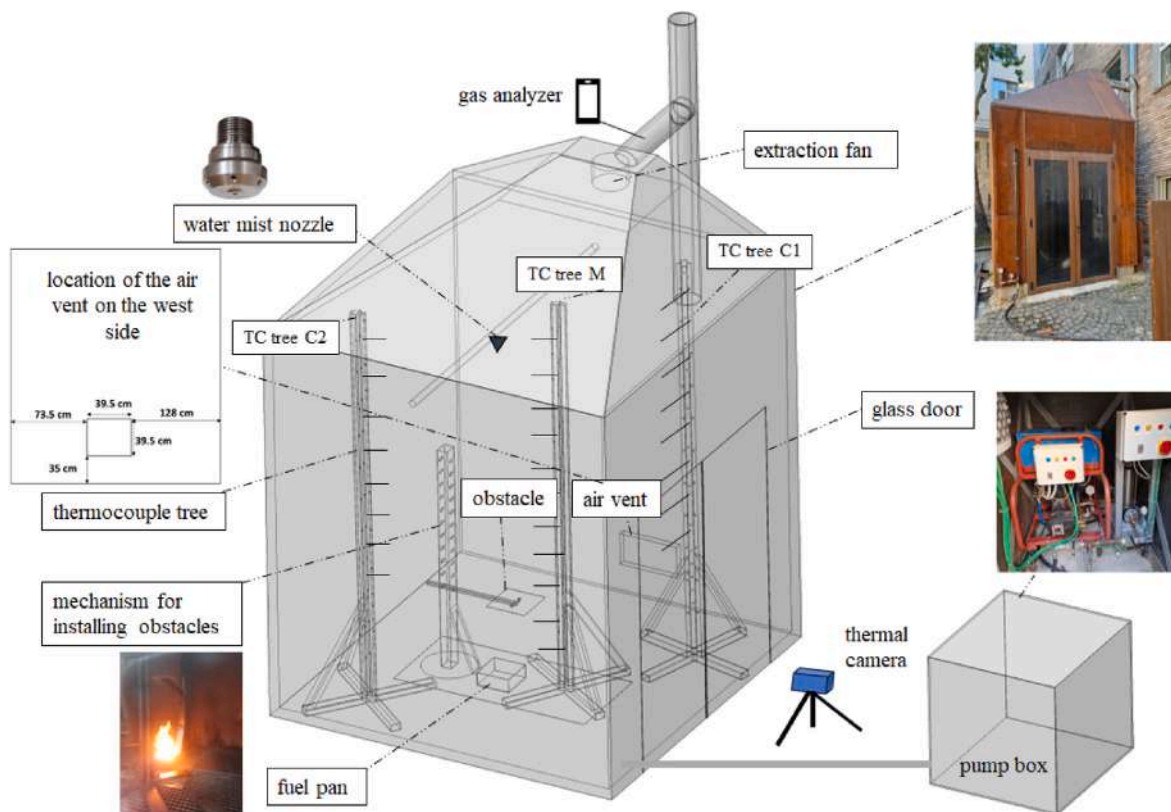


Fig. 2. Schematic of experimental set-up and apparatuses for shielded fire extinguishing tests using water mist system.

pass filter, and the downmix frequency. Moreover, the drop size and velocity values are highly sensitive to the measurement location. The parameters were selected in a way that the highest data rate could be achieved. Some of the important characteristics of the nozzle are shown in Table 4. The data were obtained for the measurement volume at 5 cm below the exit of the central injector of the nozzle.

The values of $D_{V0.5}$, $D_{V0.9}$, and $D_{V0.99}$ represent the drop diameter such that 50 %, 90 %, and 99 % of the total volume is in drops of smaller diameters, respectively. It should be noted that $D_{V0.5}$ can be referred

to as the Volumetric Median Diameter (VMD). The flow coefficient (k-factor) representing the discharge rate of the nozzle was estimated using the following equation:

$$k = \frac{Q}{\sqrt{P}} \tag{1}$$

Moreover, the distribution of the drop size and the velocity is shown in Fig. 4. A total number of 5269 measured counts were selected to report the results after validating the obtained data. The nozzle consists

Table 2
Measuring instruments.

Item	Statement	Accuracy
Thermocouple	Type K - Tersed	Probe diameter 1.6 mm: For readings up to 200 °C and between 400 °C and 1000 °C: ±0.5 °C between 200 °C and 300 °C: ±1.0 °C Probe diameter 1 mm: ±0.5 °C
Electronic weighing balance	PUE7.1.16HRP - Radwag®	Linearity: ±0.1 g Readability: 0.1 g Repeatability: 0.1 g
Data logger	HD 32.8.16 - Deltaohm	For readings up to 600 °C: ±0.1 °C Other readings: ±0.2 °C
Gas analyzer	Testo 330 - Testo	Flue gas temperature measurement: ±0.5 °C (0.0 to +100.0 °C) O ₂ measurement: ±0.2 vol % CO measurement: ±20 ppm (0–400 ppm) ±5 % of m.v. (401–2000 ppm) ±10 % of m.v. (2001–4000 ppm)
Ultrasonic flowmeter	Portaflow PF330 - Micronics	±3 % of flow reading for flow rate >0.2 m/s
Pressure gauge	16 bar - Fratelli Magni	1.6 as per EN 837-1
Thermal camera anemometer	A6753sc - FLIR® Testo 405i - Testo	- ± (0.1 m/s + 5 % of m.v.) for 0–2 m/s ± (0.3 m/s + 5 % of m.v.) for 2–15 m/s

Table 3
Details of defined cases.

Case No.	Case 0	Case 1	Case 2	Case 3	Case 4	Case5	Case 6	Case 7	Case 8	Case 9	Case 10
Obstruction size (cm²)	-	-	15 × 15	15 × 15	15 × 15	25 × 25	25 × 25	25 × 25	40 × 40	40 × 40	40 × 40
Obstacle distance from the floor (cm)	-	-	60	100	160	60	100	160	60	100	160

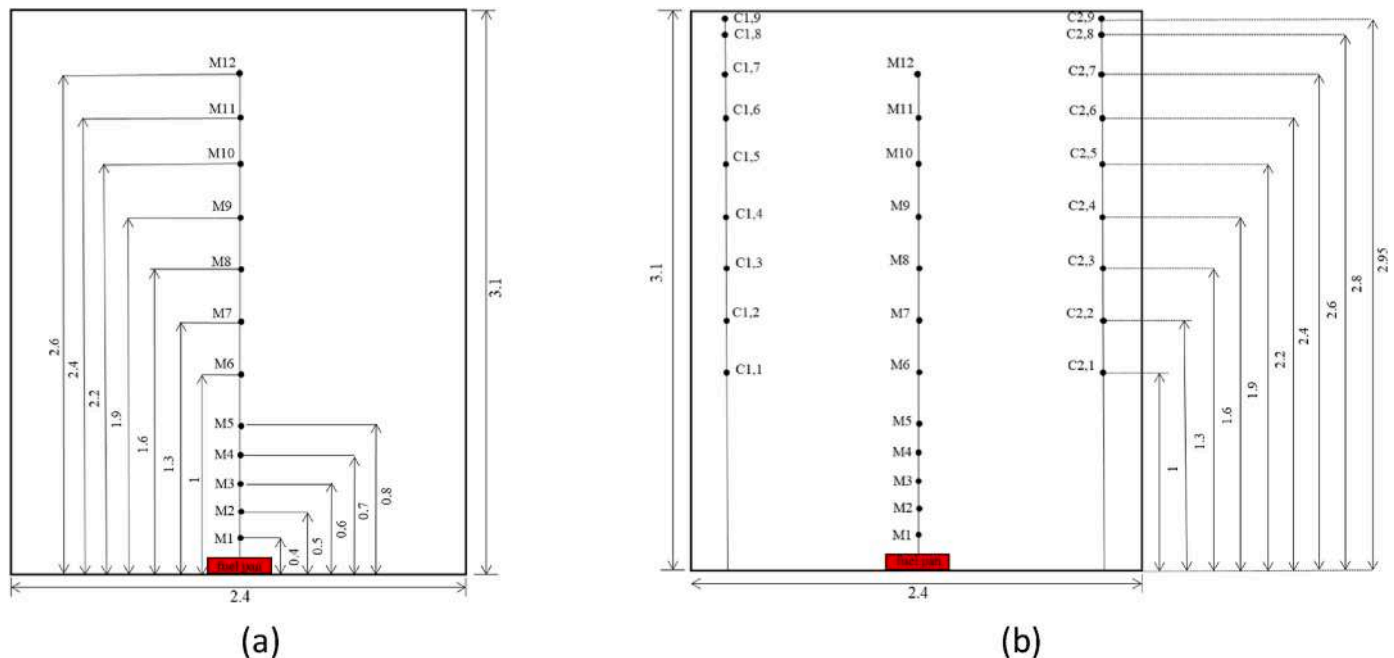


Fig. 3. Schematic of thermocouple arrangements (a) in the middle of the enclosure and (b) in the corners with 1 m offset from the central axis (measurements in m).

Table 4
Spray characteristics of the nozzle.

Pressure (bar)	Volumetric flow rate (l/min)	Mean velocity (m/s)	Flow coefficient (k factor – l/min/bar ^{1/2})	SMD (µm)	D _{V0.5} (µm)	D _{V0.9} (µm)	D _{V0.99} (µm)
10.5	18.4 ± 3 %	5.03	5.6	74.27	84.68	267.12	276.86

of an orifice oriented downward and 6 other orifices oriented at a 45° angle latitudinally and distributed at 60° longitudinally. The nozzle provides an 80° full cone angle spray pattern.

3.2. HRR measurements

Prior to the wet tests (cases 1 to 10), the Mass Loss Rate (MLR) measurements of dry tests (case 0) for two pool lengths (25 cm and 30 cm) were recorded automatically by an electronic weighing balance (PUE7.1.16HRP - Radwag®) with the maximum capacity of 16 Kg and the readability of 0.1 g which was placed below the fuel pan. The mass loss rate was recorded and transferred to a computer during each test. For MLR measurements, the tests (case 0) were also repeated at least 3 times. The equation below can be used to estimate the HRR (indicating the power of the fire) using the obtained mass loss rate. The combustion efficiency (ϕ) in this study was estimated to be 0.75 approximately. Some typical properties of diesel fuel are listed in Table 5.

$$\dot{Q} = \phi \times \dot{m}_{fuel} \times \Delta H_c \tag{2}$$

The mean mass loss rate per unit area (\dot{m}) for fuel pan 1 (25 cm × 25 cm) was 0.011 kg/m².s. The mean HRR for pool pan 1 was estimated to be 21.54 kW with a peak value of 33.09 kW. Considering only the fully developed stage approximately from 60 s to 240 s, the mean HRR value reached 26.53 kW at this stage. A thermocouple was placed above the pool pan close to the fuel surface (6 cm above the upper edge of the pan)

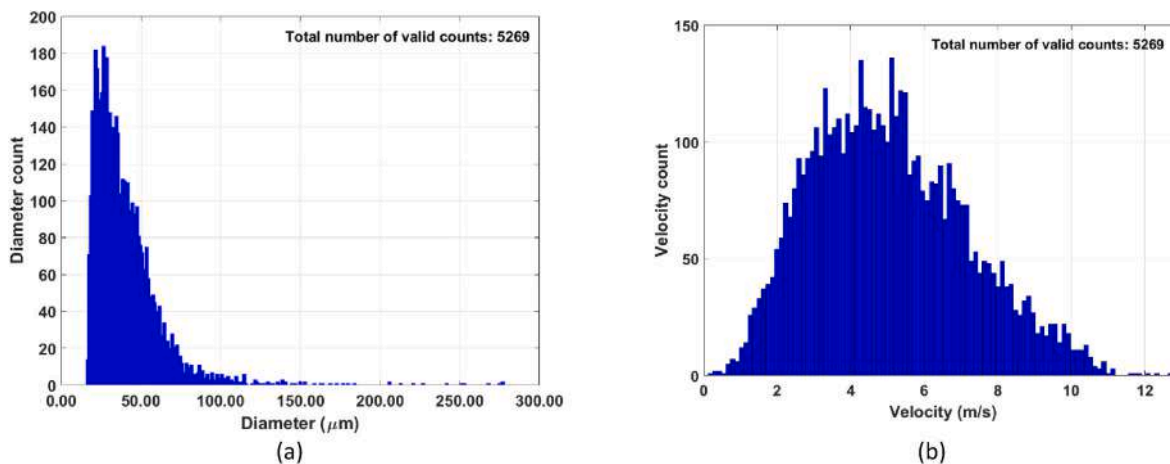


Fig. 4. Histogram of (a) the drop diameter, and (b) the drop velocity distributions.

Table 5

Typical properties of diesel fuel.

Fraction of Carbon (%)	Fraction of Hydrogen (%)	Density (kg/m ³)	Heat of combustion (MJ/kg)	Thermal conductivity (W/m.K)	Specific heat (kJ/kg.K)	Flash point (°C)
85-88 [36]	11-14 [36]	810	42.7 [37]	0.15 [38]	2.1 [37]	65.6 [36]

to record the flame temperature during the HRR measurements. The variation of the temperature with time along with the HRR evolution is depicted in Fig. 5. The temperature could reach more than 600 °C during the experiment. The fire tests lasted less than 6 min on average until burning out completely.

The mean MLR per unit area for the second pool pan (30 cm × 30 cm) was estimated to be 0.013 kg/m².s. The mean HRR and the peak HRR values were 38.65 kW and 61.70 kW, respectively. The mean HRR value for the fully developed phase approximately from 75 s to 255 s was around 45.18 kW. The estimated HRR values for both pool sizes are consistent with the reported data in Ref. [29]. The flame temperature and HRR evolutions can be seen in Fig. 6. The maximum temperature measured by the closest thermocouple to the fuel surface for this case could get to more than 600 °C.

3.3. Fire extinguishing mechanisms and suppression time

In this section, the suppression time for different cases is discussed

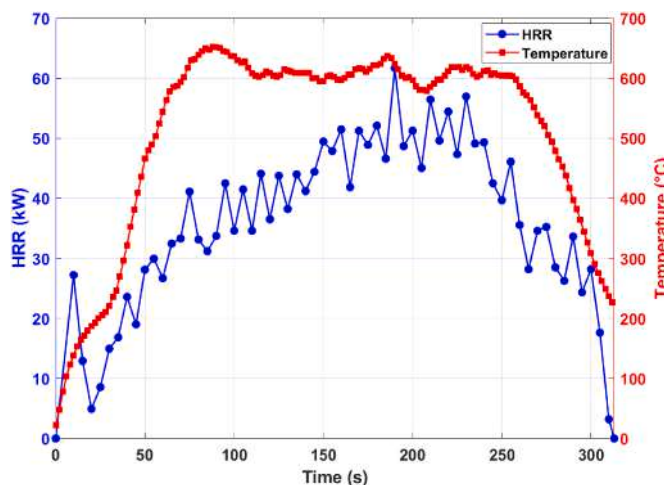


Fig. 6. HRR and temperature evolution for pool pan 2 (30 cm × 30 cm).

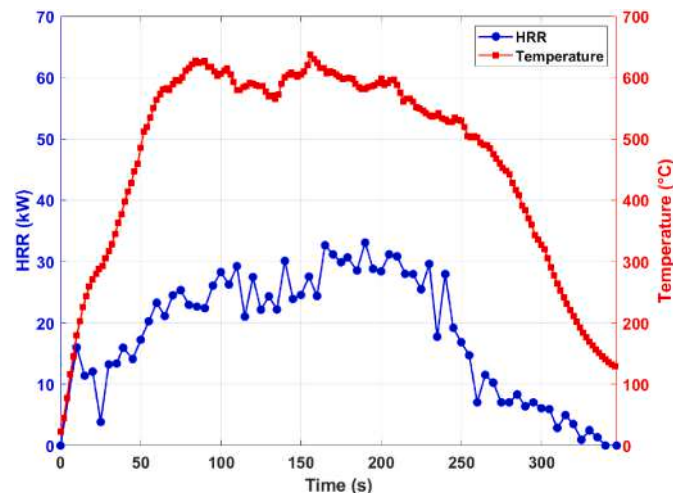


Fig. 5. HRR and temperature evolution for pool pan 1 (25 cm × 25 cm).

and compared. The nozzle was activated 150 s after ignition when using fuel pan 1 with the HRR value of about 25 kW at the time of activation. The nozzle activation time for the tests using pool pan 2 was 90 s, and the HRR was about 40 kW. The suppression time was considered as the time that no flame could be observed by the naked eye. The details of the mean suppression time for all cases with different HRRs are reported in Table 6. The water mist system was deactivated immediately after the extinguishment in successful cases, however, in any case, the maximum activation time did not exceed 1 min. In Fig. 7, the comparison of suppression time between the same cases with different HRRs and between the scenarios with the same obstacle size at different altitudes can be seen. The suppression time of case 1 (no existence of obstacle) for both pool fires was almost the same. The mist system failed to extinguish the shielded fires when the obstruction was the largest (40 cm × 40 cm) and located at 0.6 m and 1 m above the floor.

Generally, the mist system was able to extinguish the smaller pool fire in a shorter time compared to pool fire 2 except case 6 in which the larger pool fire was not completely covered by the obstacle and the mist

Table 6
Details of the extinguishing times.

Case No.	1		2		3		4		5		6		7		8		9		10	
Extinguishing time (s)	Pan		Pan		Pan		Pan		Pan		Pan		Pan		Pan		Pan		Pan	
	I	II	I	II	I	II	I	II	I	II	I	II	I	II	I	II	I	II	I	II
	4	4.5	8.8	11	6	9.5	5	9.6	49	58	27	23.5	6	22	failed	failed	failed	failed	34	53

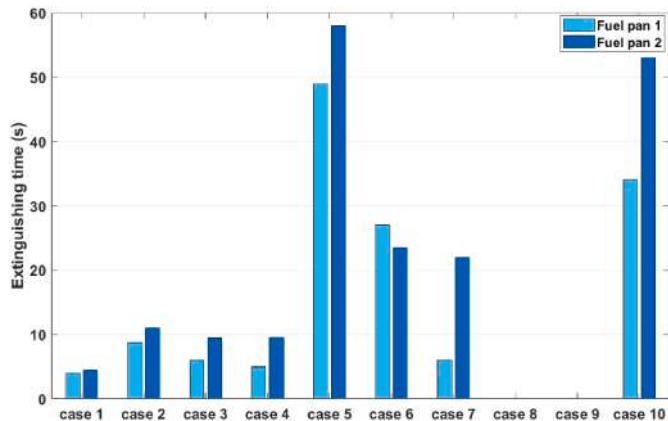


Fig. 7. Comparison of extinguishing time of all cases.

droplets could reach the fuel surface. By comparing cases with the same obstacle distance from the nozzle, the fire suppression time increased by the enhancement of the obstacle size. The fire extinguishing time decreased by reducing the distance between the obstruction and the nozzle in cases with the same obstacle size. The effect of shielding conditions on the suppression time will be discussed in the next sections.

The combustion behavior and different phases of the burning process and extinguishing process visualized by a thermal camera are shown in Fig. 8 for some selected cases. Each set of pictures consists of 10 photos in which the first 5 pictures represent the burning process before the water mist discharge including the fire growth and the fully developed stages. The activation time of each case is indicated in the fifth picture, and the last 5 photos display the decay and suppression phase after nozzle application. In the last picture of each case, the extinguishing or burn-out times are shown. The interaction between the mist droplets and the flames can be clearly seen from the sixth picture onward, and the fire extinguishing mechanisms can be diverse for each case depending on the shielding conditions. In case 1, the fire was completely exposed to the

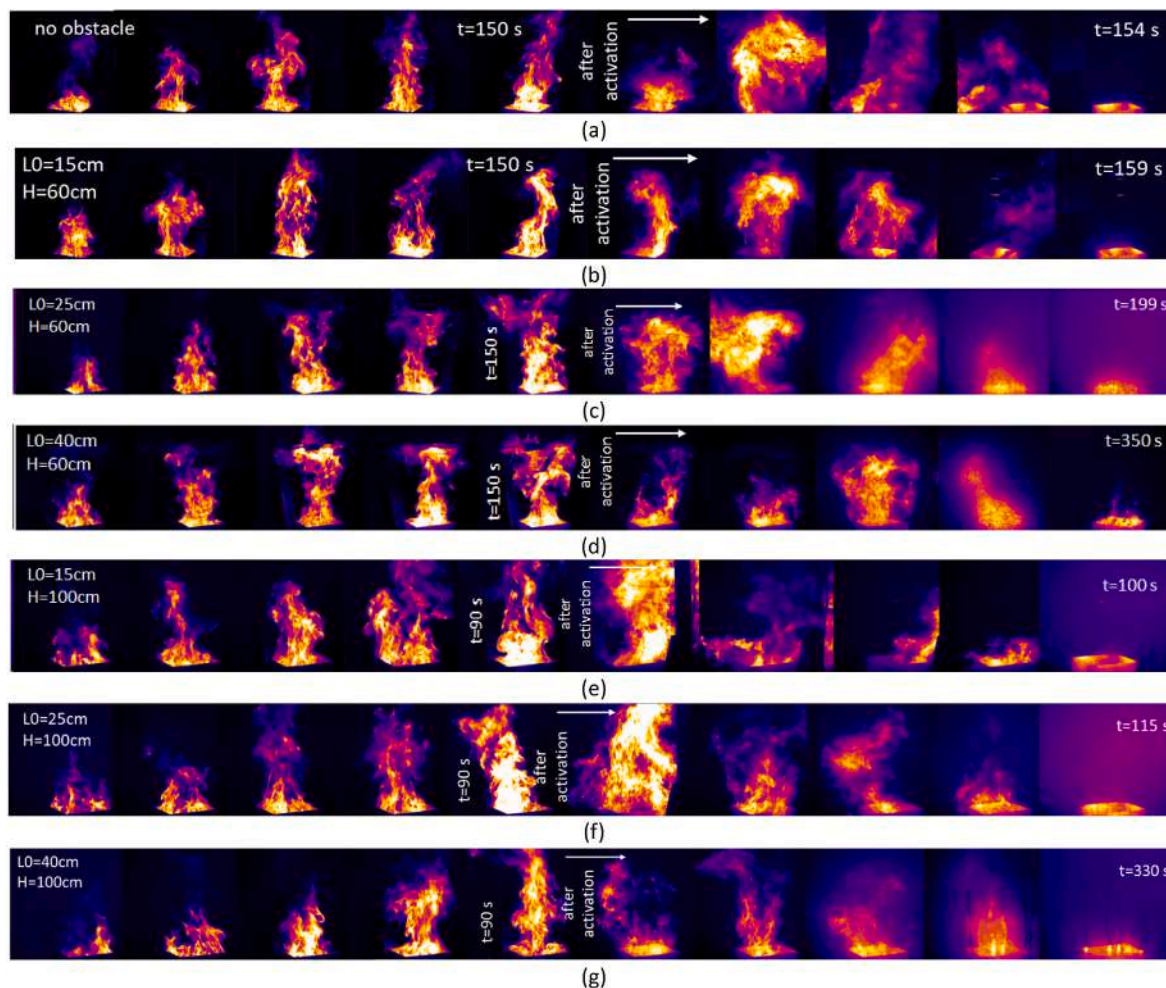


Fig. 8. Photographs taken by the thermal camera representing different stages of the burning process using pool pan 1: (a) case 1, (b) case 2, (c) case 5, and (d) case 8, and using pool pan 2: (e) case 3, (f) case 6, and (g) case 9.

mist droplets and therefore it was suppressed in a short time through the fuel and flame cooling and evaporation. Other sets of photos display sheltered fire scenarios with three obstacle sizes located at the same height (cases 2, 5, and 8 for fuel pan 1 and cases 3, 6, and 9 for fuel pan 2). When the obstruction was larger, the chance of mist droplets reaching the fire plume and flames was lower; however, some droplets could bypass the obstacle and suppress the fire like in cases 2 and 5 ($H = 60$ cm, pan 1) or cases 3 and 6 ($H = 100$ cm, pan 2). The shielded fire in cases 8 and 9 was surrounded by the droplets, but the droplet penetration to the flames was not enough to extinguish the fire completely due to the large obstacle. In shielded fire scenarios, some droplets hit the obstruction and they can integrate and make coarser droplets which lead them to move along the underside of the obstacle and then drop down to the fuel surface. Also, some droplets can directly reach the flame and the fuel surface. The interaction between the coarser droplets and the fuel surface can cause cracking sounds sometimes. Moreover, in cases where the fire was not extinguished like in case 9 using the second pool pan, the mist application could sometimes intensify the fire and consequently, more smoke was produced after the mist application.

All the fire extinguishing mechanisms can be involved in the shielded fire suppression scenarios to some extent with respect to the shielding condition. In cases where the fire source is not fully covered by the obstruction, some droplets can reach the flame and extract heat while coarser droplets can penetrate the flame region, reach the fuel surface, and interrupt the fuel vaporization process. The combustion chain reaction is also interrupted by mist droplets. Oxygen displacement and thermal radiation attenuation are the other mechanisms involved in the shielded fire extinguishing process.

3.4. Temperature distribution and gas concentration

The temperature and gas concentration evolutions in the enclosure are presented and compared for different shielded fire scenarios. Fig. 9 (a) to (c) represent the variation of M1 temperature with time for each 3 cases with the same obstruction size and diverse obstacle height along with the results for case 0 and case 1 for fuel pan 1. It should be noted that the case number and the shielding conditions (obstruction size and height) of each curve are mentioned in the legend of the plots. The water mist nozzle was activated 150 s after ignition when the HRR was around 25 kW. As shown in Fig. 9 (a), the fire was not fully sheltered by the obstacle ($15\text{ cm} \times 15\text{ cm}$) in cases 2–4, therefore, mist drops could reach the flame or the fuel surface. M1 temperature could get to around $400\text{ }^\circ\text{C}$, and it dropped down sharply after nozzle activation until it reached the ambient temperature (cases 1, 3, and 4). The temperature reduction in cases 1 and 4 followed almost the same trend. However, the temperature decay was prolonged in case 2 as the obstacle was placed closer to the fire source.

As can be seen in Fig. 9 (b), M1 temperature in case 5 kept increasing after nozzle activation for a few seconds and then decreased gradually. The temperature variation in case 6 was almost the same as in case 5, but the temperature decay was quicker after activation. The temperature reduction in case 1 (no obstacle) and case 7 where the obstacle was closer to the nozzle was almost identical. The temperature evolutions in cases 8–10 are displayed in Fig. 9 (c). As the water mist system failed to suppress the shielded fire in case 8, the temperature fluctuation followed almost the same tendency as in case 0 (dry test). There was no fire extinguishment also in case 9, however, the temperature decay was quicker than that of cases 0 and 8. By comparing the suppression time

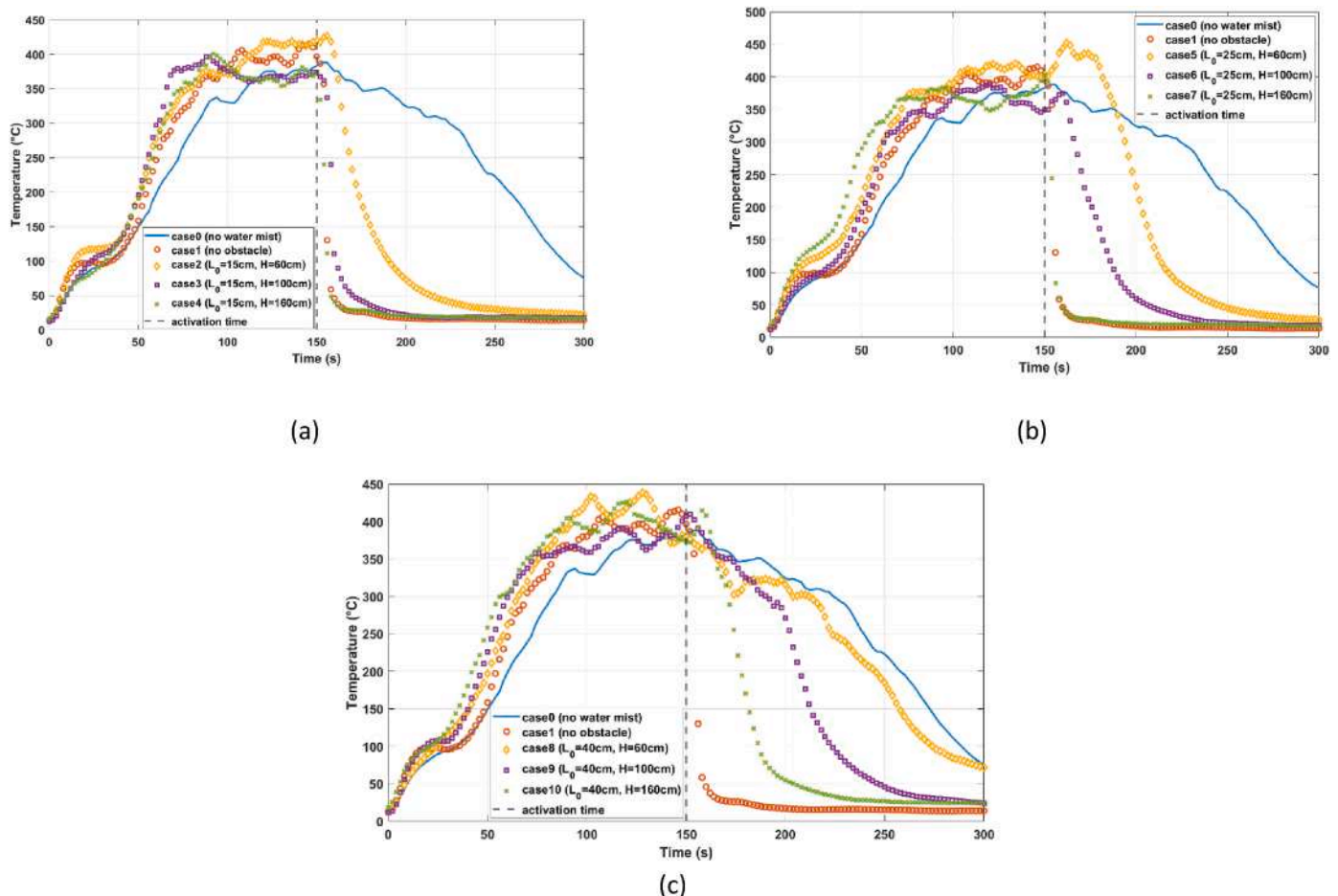


Fig. 9. Comparison of M1 temperature evolution between case 0, case 1, and (a) cases 2 to 4 (b) cases 5 to 7, and (c) cases 8 to 10 using fuel pan 1.

and the temperature evolution of shielded cases with the same obstacle distance from the nozzle and diverse obstacle size, it can be seen that generally, the larger obstruction leads to the longer suppression time and temperature decay. However, the trend of the temperature decrease in cases 4 and 7 ($H = 160\text{ cm}$) using the first pool pan was almost the same due to the fact that in both cases, the obstacles at that distance were not large enough to completely block the mist droplets. It is worth noting that although the obstruction in case 10 was larger than in case 5, the suppression time and consequently the temperature reduction was shorter. This indicates the importance of the obstruction distance from the nozzle or from the fire source in affecting the performance of the water mist system.

The same plots of M1 temperature variations for the second pool pan ($30\text{ cm} \times 30\text{ cm}$) fire tests are presented in Fig. 10 (a) to (c). The activation time of the water mist system was 90 s after ignition when the HRR was around 40 kW. As displayed in Fig. 10, M1 temperature increased up to more than $500\text{ }^\circ\text{C}$ before nozzle application for all cases. The temperature decreased promptly to the ambient temperature in cases 1, 3, and 4 after nozzle application. However, the temperature in case 2 increased after mist activation for a few seconds and then decreased sharply (Fig. 10a). The same scenario of temperature reduction occurred for cases 5 to 7 (Fig. 10b). The descending trend of the temperature reduction after nozzle activation in cases 6 and 7 was

slower than that of cases 3 and 4. However, the M1 temperature in case 5 enhanced first after nozzle application and then declined to the ambient temperature steadily. M1 temperature evolutions for cases 8 to 10 are shown in Fig. 10c. As explained in the previous section, the mist nozzle failed to put off the fire in cases 8 and 9, therefore, it can be seen that the temperature decreased slightly after water mist activation and then increased gradually to its maximum value due to the fire intensification by water mist drops. Then, the temperature dropped down gradually as the fuel burnt out. In case 10, the temperature reduced slightly after using the water mist system but then declined steadily due to the successful fire extinguishment.

As mentioned before, the lateral temperature measurements were conducted by 2 thermocouple trees in the corners with 1 m offset from the central axis with 18 thermocouples positioned at different altitudes. In order to avoid repetition, only the temperature values obtained by the second thermocouple tree (C2,1 – C2,9) are represented here. Fig. 11 (a) – (c) show the temperature rise in the corner of the compartment at different heights and times (before and after nozzle activation) for cases 0 to 10 using pool fire 1. It should be noted that the ambient temperature was subtracted from the C temperatures for all cases. The temperature difference between the upper and lower layers in the enclosure could reach more than $10\text{ }^\circ\text{C}$. The C temperature rise for all cases fluctuated between $20\text{ }^\circ\text{C}$ and $40\text{ }^\circ\text{C}$ approximately before using the mist spray at t

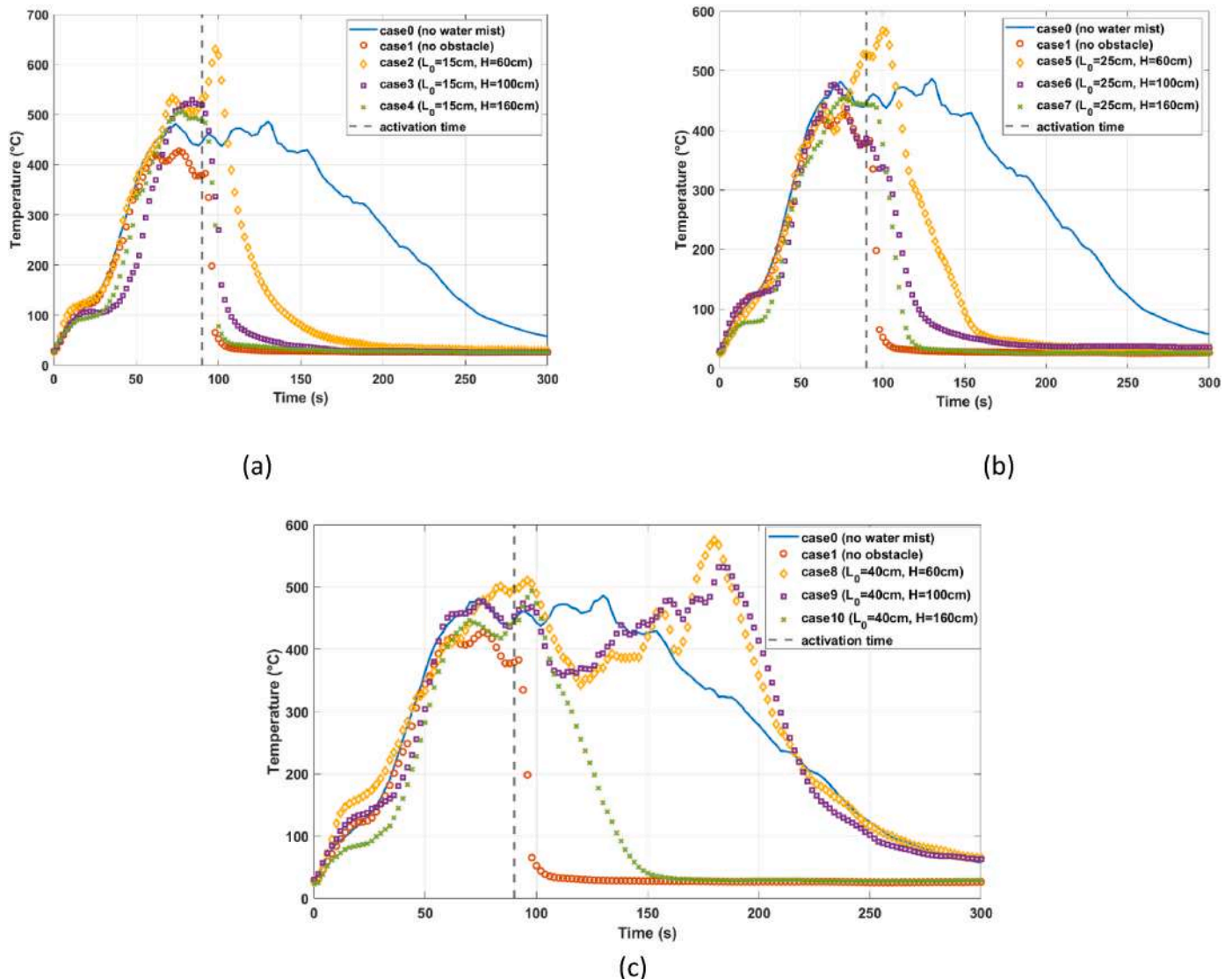


Fig. 10. Comparison of M1 temperature evolution between case 0, case 1, and (a) cases 2 to 4 (b) cases 5 to 7, and (c) cases 8 to 10 using fuel pan 2.

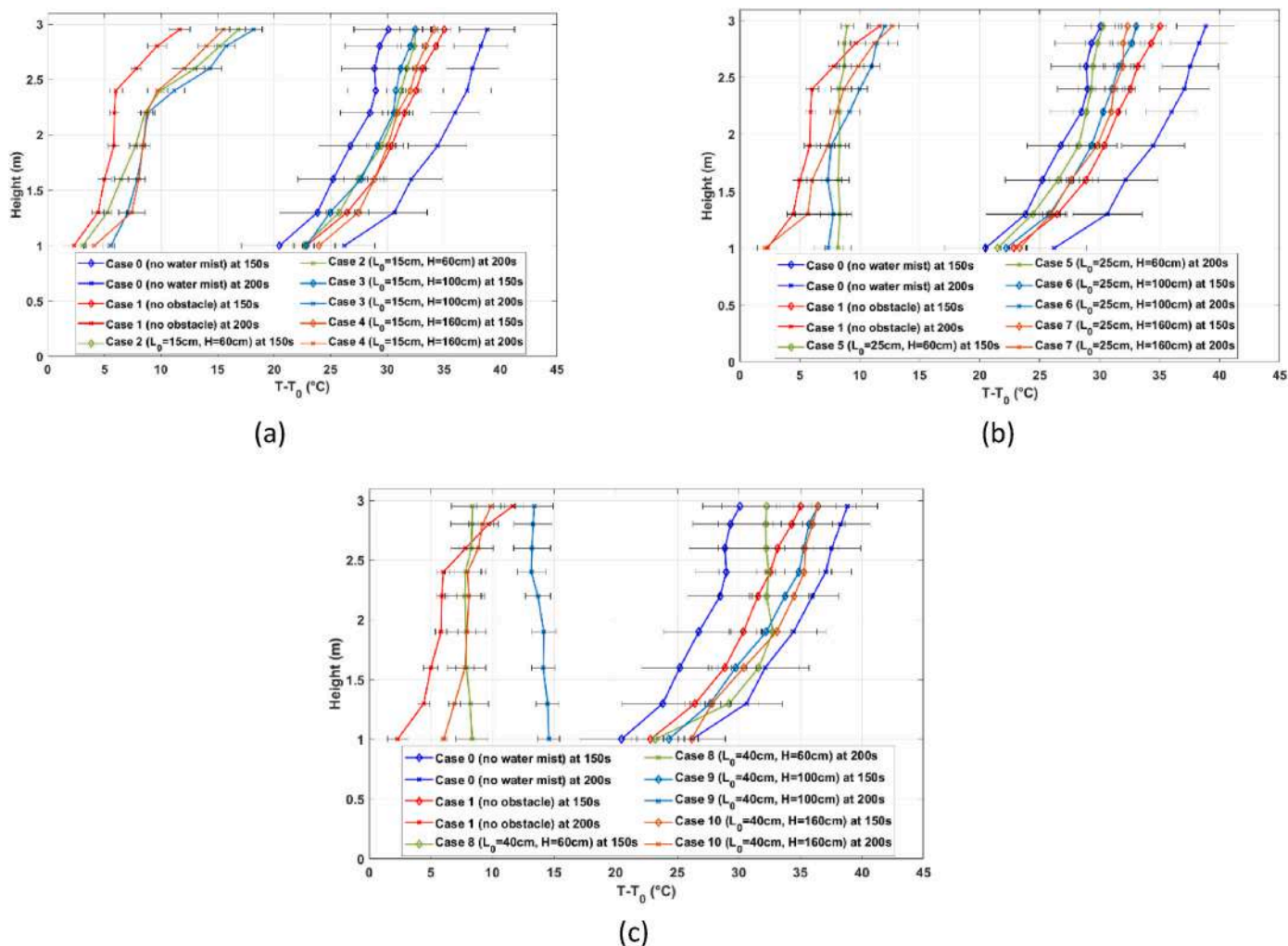


Fig. 11. Lateral temperatures (C2, 1 – C2,9 thermocouples) at different heights at $t = 150$ s (before nozzle activation) and $t = 200$ s (50 s after nozzle activation) using the first fuel pan for cases 0, 1, and (a) 2–4, (b) 5–7, and (c) 8–10.

= 150 s. However, the water mist system was able to decrease the lateral temperature significantly after 50 s of water discharge even in unsupported cases ($t = 200$ s).

The lateral temperature (C2,1 – C2,9) variations with height for the fire tests with the second fuel pan are displayed in Fig. 12 (a) – (c). The temperature rise evolutions for all cases are plotted at two different times; at $t = 90$ s before activating the water mist system and at $t = 140$ s, 50 s after nozzle application. The temperature at C2,9 thermocouple in case 0 (dry test) could rise to almost $70\text{ }^{\circ}\text{C}$ at $t = 140$ s. The lateral temperatures reached higher values compared to the previous cases and the temperature increased by almost $40\text{ }^{\circ}\text{C}$ at the highest altitude before nozzle activation. The temperature reduction after mist application fluctuated approximately between $0\text{ }^{\circ}\text{C}$ and $20\text{ }^{\circ}\text{C}$ at different altitudes. Overall, by comparing the lateral temperatures between case 0 and other cases, it can be seen that the water mist system could decrease the temperature significantly. Therefore, the water mist nozzle was successful in controlling the lateral temperature even in failed suppression cases.

The exhaust gas analysis for all cases using the first fuel pan is performed based on the data shown in Fig. 13 (a) – (c). The production of carbon monoxide is generally dependent on the extinguishing time. The longer water discharge time in cases with a longer extinguishing time or in burning-out cases leads to the longer duration of CO production due to incomplete combustion. As shown in Fig. 13, the CO concentration enhanced gradually from the ignition until nozzle activation. Then, the

CO production increased sharply after discharging for cases in which some droplets could reach the fuel surface. For instance, the enhancement of CO concentration after nozzle activation in cases 2 to 4 (small-size obstruction) was sharper than those of cases with larger obstacle (cases 8 to 10). However, the CO production duration was longer for cases 5 and 8 to 10, due to the longer combustion time. The oxygen concentration decreased steadily from the ignition to the activation time, then continued dropping down steadily after nozzle activation. The longer extinguishing time led to more consumption of oxygen. The oxygen concentration increased after burning-out or fire suppression. The CO concentration could reach a maximum value of 150 ppm in case 5 because of the longer nozzle application time.

The same gas concentration analysis for cases 1–10 using fuel pan 2 is carried out and the results are displayed in Fig. 14 (a) – (c). The maximum CO concentration (225 ppm) in case 0 was much higher than that of case 0 using the smaller pool pan, and the oxygen concentration dropped down to the minimum value of around 19 %. As discussed before, the longer time of mist application could lead to more production of CO and more consumption of oxygen in the enclosure. This is also valid for all cases reported here. After nozzle activation, a sharp increase of carbon monoxide and a sharp decrease of oxygen can be identified. The production of CO in cases 8 and 9 reached more than 200 ppm as the water mist was activated for 1 min and failed to extinguish the fire.

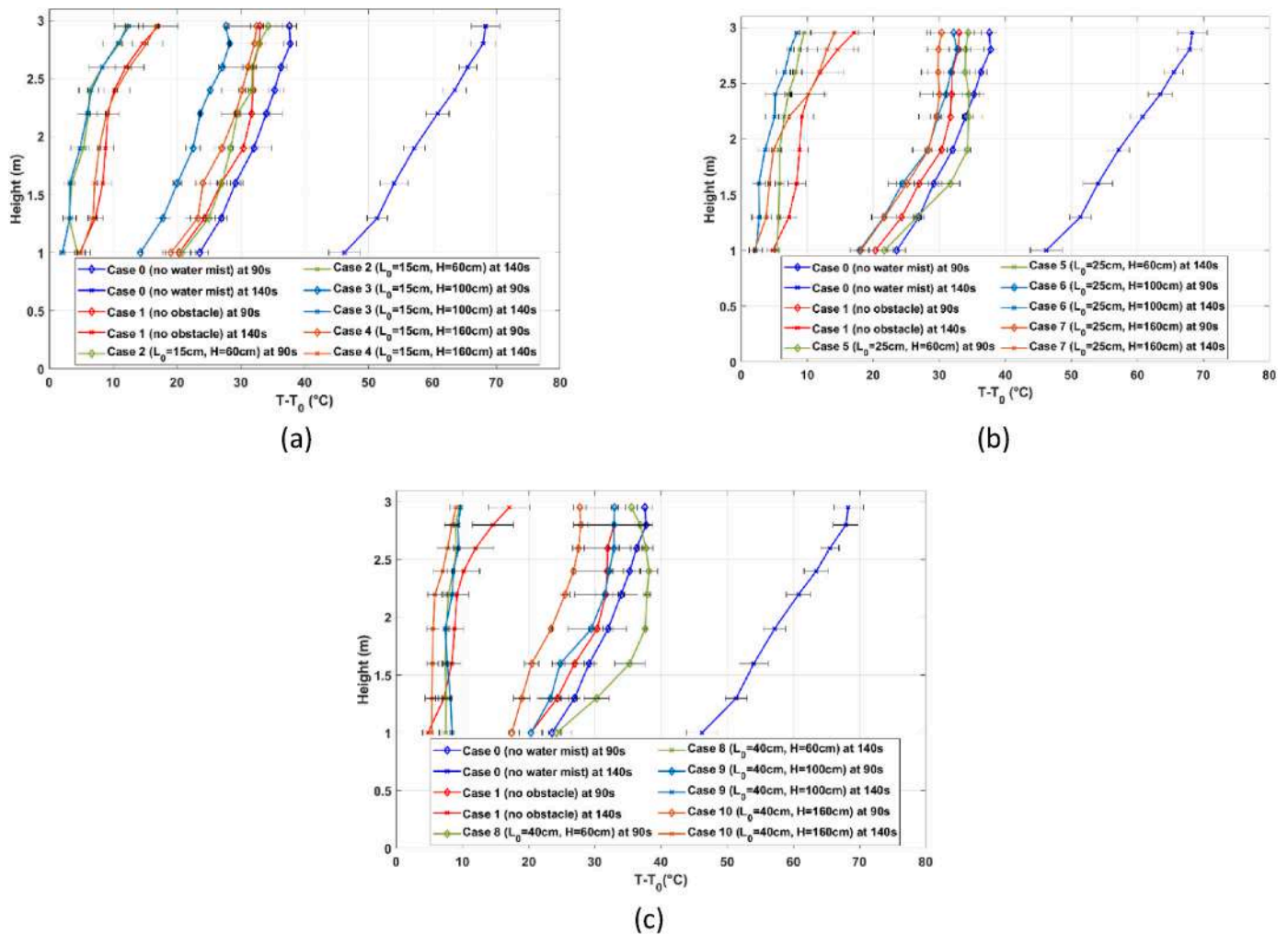


Fig. 12. Lateral temperatures (C2, 1 – C2,9 thermocouples) at different heights at $t = 90$ s (before nozzle activation) and $t = 140$ s (50 s after nozzle activation) using the second fuel pan for cases 0, 1, and (a) 2–4, (b) 5–7, and (c) 8–10.

3.5. Impact of shielding conditions and plume-spray interaction

As shown before, the existence of obstacles in realistic fire scenarios can affect the performance of water mist systems significantly. In this section, the impact of different shielding conditions including the obstruction size and its distance from the nozzle is discussed in more detail. In order to characterize the effect of shielding conditions, it is necessary to define some terms including a block ratio and a plume-spray thrust ratio. As defined by Liu et al. [28], the block ratio represents the geometric projection and the blocking effect of the obstacle, and it can be estimated by the following equation [28]:

$$kp = \frac{L_p}{L_f} = \frac{hL_0}{h_s L_f} \quad (3)$$

It should be noted that the spray angle should be wider than θ_0 , which is the angle formed by the mist spray and the obstacle. The geometric parameters in this formula are displayed in Fig. 15. This equation shows the projection length of the mist spray to the fuel pan surface formed by the obstacle divided by the length of the fuel pan. The characteristics of each case and the geometric parameters including the block ratio for both pool fires are summarized in Table 7.

As reported in Table 7, the block ratio increased with the reduction of the distance between the obstacle and the nozzle for the cases with the same obstruction size. Based on the interaction between the mist droplets and the buoyant fire-induced plume [30], the plume-spray thrust

ratio is defined to demonstrate how spray thrust can overcome the plume thrust in order to quantify the penetration of the droplets into the fire zone. This is a complex phenomenon and only a few research studies attempted to explain and characterize this phenomenon including [8, 39]. Liu et al. [40] suggested that the spray momentum should be at least equal to the fire plume momentum to prevent the droplets from being carried away, while in Ref. [29], a critical plume-spray thrust ratio of 5 was proposed. In the experiments of Downie and Polymeropoulos [41], they reported a large plume-spray thrust ratio resulting in lower droplet penetration into the fire zone (in the range of 5–10). Santangelo et al. [42] employed a method to quantify the thrust force of the spray by measuring the water weight with a load cell placed below the nozzle. The plume-spray thrust ratio should be in a range that the spray droplets can penetrate the plume region, otherwise, the droplets will be carried away. The plume-spray thrust ratio and other equations suggested by Refs. [29,43–45] are as follows:

$$\alpha = \frac{F_f}{F_w} \quad (4)$$

The momentum of the fire plume (F_f) and the momentum of spray (F_w) are as follows:

$$F_f = \dot{m}_p \cdot u_0 \quad (5)$$

$$F_w = \dot{V} \cdot U_0 \quad (6)$$

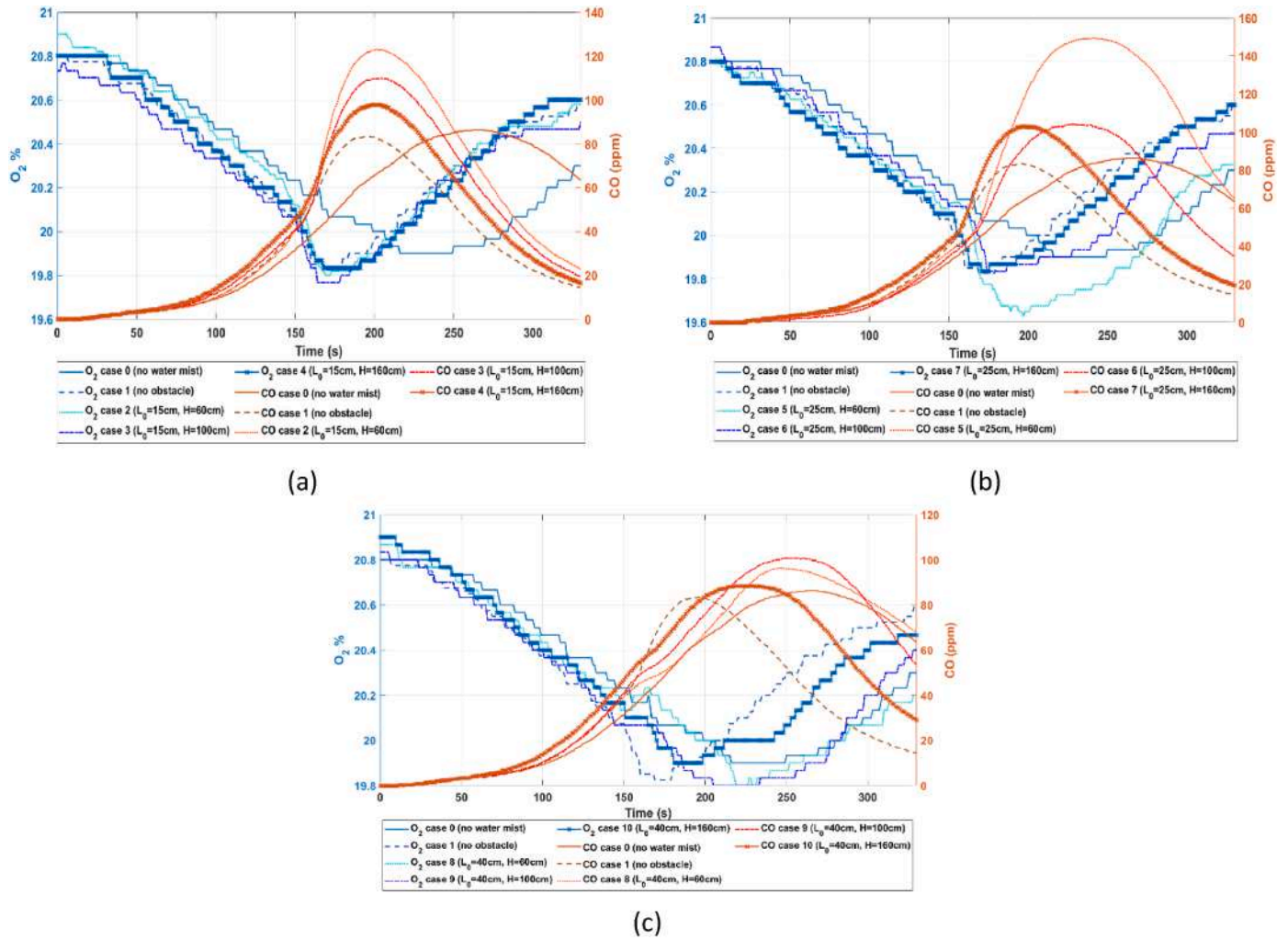


Fig. 13. CO and O₂ concentrations (mean values) in the exhaust chimney for cases 0, 1, and (a) 2 to 4 (b) 5 to 7, and (c) 8 to 10 using fuel pan 1.

Where \dot{m}_p and u_0 are given by:

$$\dot{m}_p = 0.071 \dot{Q}_c^{1/3} \cdot (z - z_0)^{5/3} + 1.92 \cdot 10^{-3} \cdot \dot{Q}_c; \text{ for } z > L \quad (7)$$

$$\dot{m}_p = 0.0056 \dot{Q}_c \frac{z}{L}; \text{ for } z < L \quad (8)$$

$$u_0 = 1.1 \left(\frac{z}{\dot{Q}_c^{2/5}} \right)^{-1/3} \cdot \dot{Q}_c^{1/5} \quad (9)$$

$$L = 0.235 \dot{Q}_c^{2/5} - 1.02 L_f \quad (10)$$

$$z_0 = 0.083 \dot{Q}_c^{2/5} - 1.02 L_f \quad (11)$$

It should be noted that the above-mentioned equations may not provide a complete explanation of what really happens in the interaction area between the droplets and the fire plume. In these equations, it is assumed that all the water spray mass moves vertically with an average velocity; however, in reality, depending on the spray pattern, some droplets may have a different vertical velocity magnitude. Larger droplets have greater momentum allowing them to penetrate the plume region and reach the fuel surface. Another point to notice is that the existence of obstacles, especially larger ones may affect the upward fire plume momentum. In this regard, further experiments seem necessary to develop more accurate formulations for the fire plume momentum of the shielded fire scenarios. Moreover, the HRR is also assumed to be

constant and not vary remarkably with time. In the current work, the thrust force of the spray was estimated by multiplying the droplet velocity (U_0) obtained by the PDPA system and the water discharge rate (\dot{V}) measured in the tests (these values were reported in the previous section). Since the working pressure of the nozzle was the same in all tests, the momentum of the spray was considered constant, thus, the plume-spray thrust ratio increased with the HRR. The estimated fire plume thrust force ranged between 1 and 3 N at the nozzle location. The block ratio is plotted against the extinguishing time for all successfully suppressed cases, and the calculated plume-spray thrust ratio for two fire sizes is indicated in Fig. 16. The plume-spray thrust ratios were below the critical value ($\alpha = 5$) reported by Ref. [29] for small diesel pool fires. As shown in Fig. 16, when the obstacle was closer to the nozzle ($H = 100$ cm and 160 cm), more droplets had the chance to bypass the obstruction and penetrate the fire plume region leading to more evaporation and flame cooling, also some mist droplets surrounded the fire source resulting in more oxygen displacement and thermal radiation attenuation. However, this is highly dependent on the spray pattern of the nozzle and the obstacle size. By comparing the same cases between two pool fires (same h_c and L_0), it can be observed that the block ratio of the first fuel pan was greater than that of the second one for each case (decrease of L_f) and the suppression time was shorter for almost all cases. In cases with the same shield distance from the nozzle and the same fuel pan length, the block ratio and the extinguishing time were enhanced by increasing the obstacle length (increase of L_0). Overall, considering all cases with the same obstacle length for both pool

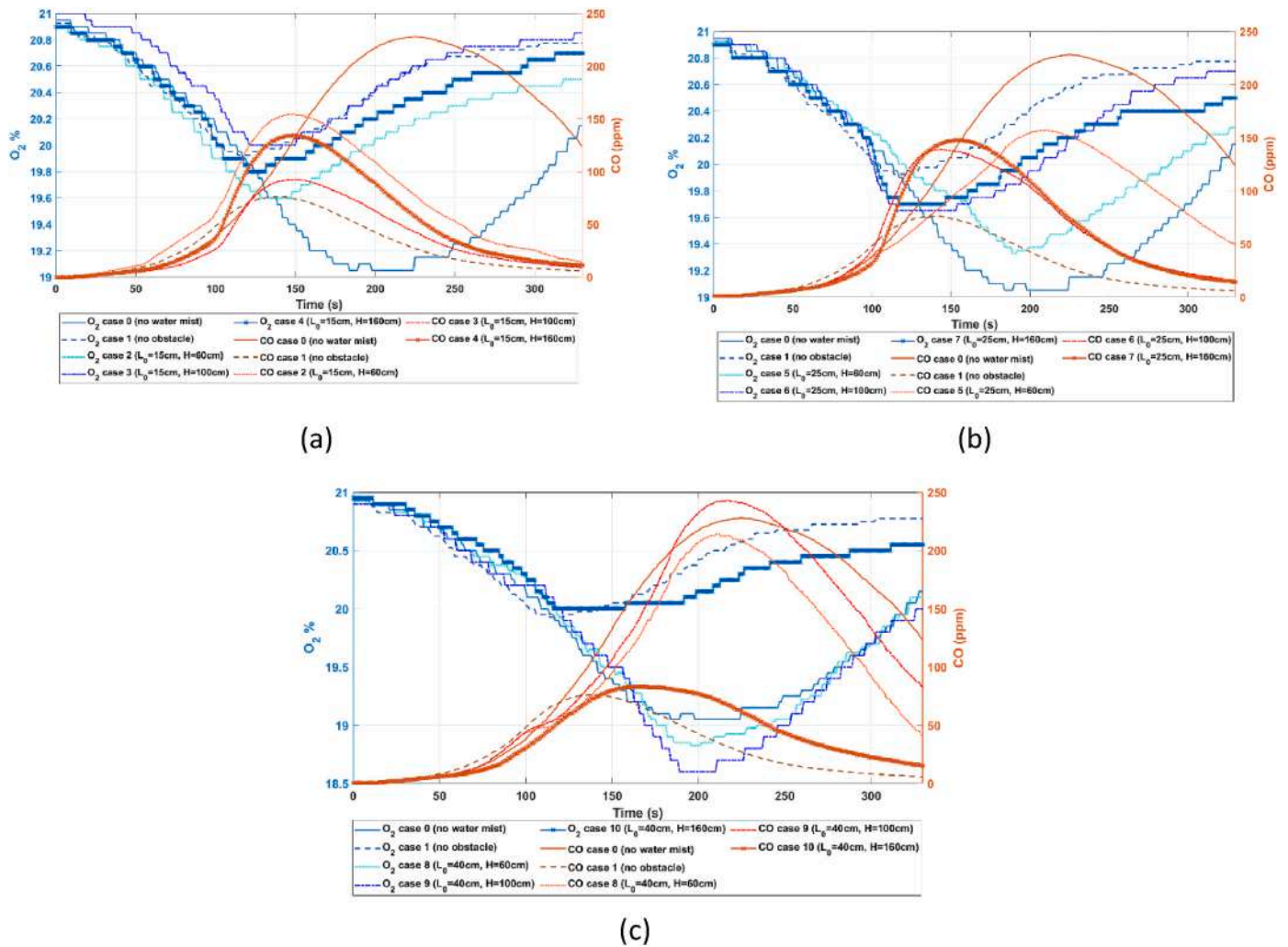


Fig. 14. CO and O₂ concentrations (mean values) in the exhaust chimney for cases 0, 1, and (a) 2 to 4 (b) 5 to 7, and (c) 8 to 10 using fuel pan 2.

fires, it can be seen that the suppression time decreased almost linearly by increasing the block ratio in cases 5 to 7. The same behavior can also be observed in cases 2 to 4 with the obstacle size of 15 cm. In order to evaluate the results for the largest obstacle (40 cm), the burning time for case 9 in the first pool fire tests is also displayed in Fig. 16. The reported burning time for case 9 is the average of the suppression time in successful tests and the burning time in failed tests. The increase of the block ratio in cases 8 to 10 also led to a reduction in the suppression time. It should be noted that the suppression performance in cases 2–4 was more dependent on the fire size than the height of the obstruction. However, the suppression time was more sensitive to the distance between the obstacle and the nozzle in cases 5–7 and 8–10.

4. Conclusions

A comprehensive experimental campaign was conducted to assess the shielded fire behavior and the capability of water mist systems to control such fire scenarios. A low-pressure water mist nozzle was used to extinguish diesel pool fires in a compartment equipped with a mechanism to provide different shielding conditions by changing the obstruction size and its distance from the nozzle. A variety of parameters were measured like the mist droplet size distribution and the downward velocity of the nozzle by a PDPA system, the temperature by thermocouples, and the gas concentrations by a gas analyzer, and the obtained results for different cases were compared and discussed in the current work. Based on the analysis, the following main conclusions emerge.

- A PDPA system was installed and calibrated to measure the droplet size distributions and the downward velocity of the low-pressure nozzle at the working pressure of 10.5 bar. The set-up parameters of the system were analyzed, and the optimum values were obtained for this specific application. Different diameter values including SMD, $D_{V0.5}$, $D_{V0.9}$, and $D_{V0.99}$, and the discharge velocity were measured and reported. These measurements can be useful for further numerical analysis or comparison studies with other water mist sprays.
- The mass loss rate of the diesel fuel was measured and recorded during the fire test in order to determine the HRR values. However, these tests were limited to dry tests only. The diesel combustion efficiency in this work was around 0.75. It was estimated that the mass loss rate per unit area, the mean HRR, the mean HRR in the fully developed phase, and the peak HRR for fuel pan 1 (25 cm × 25 cm) were 0.011 kg/m².s, 21.54 kW, 26.53 kW, and 33.09 kW, respectively. The same measurements for fuel pan 2 (30 cm × 30 cm) were 0.013 kg/m².s, 38.65 kW, 45.18 kW, and 61.70 kW in the same order.
- The water mist system successfully suppressed the shielded fire within 1 min of activation in 8 cases for both pool pans with different shielding conditions. However, the nozzle failed to control the fire in 2 cases where the obstacle was the largest (40 cm × 40 cm) and was placed closer to the pool fire (at h = 0.6 m and 1 m). Generally, the suppression time increased with the fire and the obstacle size and

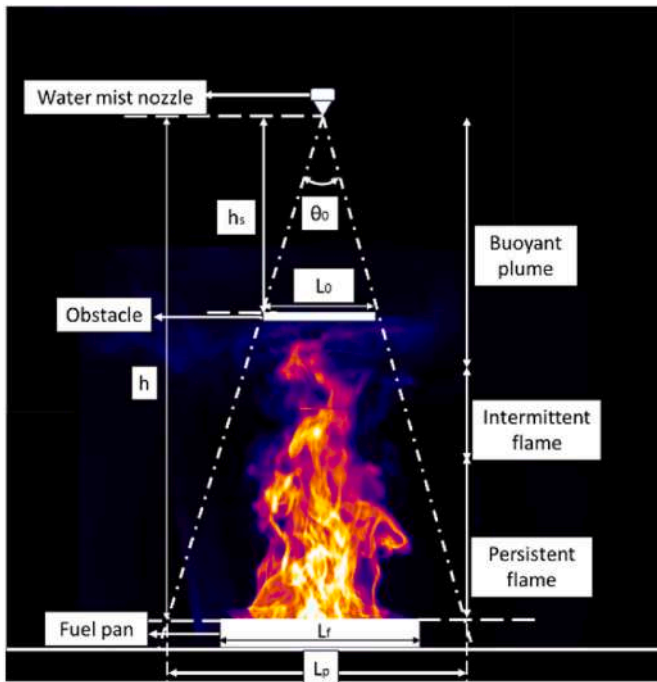


Fig. 15. Schematic view of the geometric projection definitions in a shielded fire scenario (adapted from Ref. [28] with permission).

decreased by reducing the distance between the nozzle and the obstruction.

- Depending on the shielding condition, the fire extinguishing mechanisms can be diverse. In cases where the fire was completely exposed to the droplets or in cases where the fire was partially covered by the obstruction, the mist droplets could extinguish the fire mainly through the endothermic cooling as some mist droplets could bypass the obstacle and reach the flames and the fuel surface. The mist drops could interrupt the combustion chain reaction and fuel vaporization process.
- According to the temperature distribution outputs, M1 temperature declined quickly after nozzle activation in cases with short suppression time (i.e., cases 1, 3, 4, and 7 for fuel pan 1 or cases 1, 3, 4, 6, and 7 for fuel pan 2). On the contrary, in some other cases (i.e., cases 2 and 5 for both fuel pans) the temperature first increased sharply

after activation and then declined steadily. The water mist system could not affect the temperature evolution in failed suppression cases and the temperature kept fluctuating until burning-out. M1 temperature after nozzle activation in cases 8 and 9 (pool pan 2) increased gradually after a few seconds of reduction, due to the fire intensification. Moreover, the lateral temperatures declined significantly after nozzle application in all cases.

- The variation of carbon monoxide production was dependent on the fire extinguishing time. Due to incomplete combustion, the production of CO increased sharply after water discharge in all cases. The oxygen concentration followed a descendent trend after activation until suppression or burning-out. Generally, longer suppression time led to more oxygen consumption and longer CO production.
- The geometric projection of obstacles was quantified by a block ratio. In cases with the same obstacle size, the block ratio increased with decreasing the distance between the spray and the obstacle and the suppression time declined. A plume-spray thrust ratio can be defined to analyze the capability of the spray penetration into the fire zone by estimating the fire-induced plume and spray thrust forces. The calculated plume-spray thrust ratios were less than the critical ratio proposed by Ref. [29].
- The investigation of the performance of the low-pressure and high-pressure water mist nozzles with different working pressures for

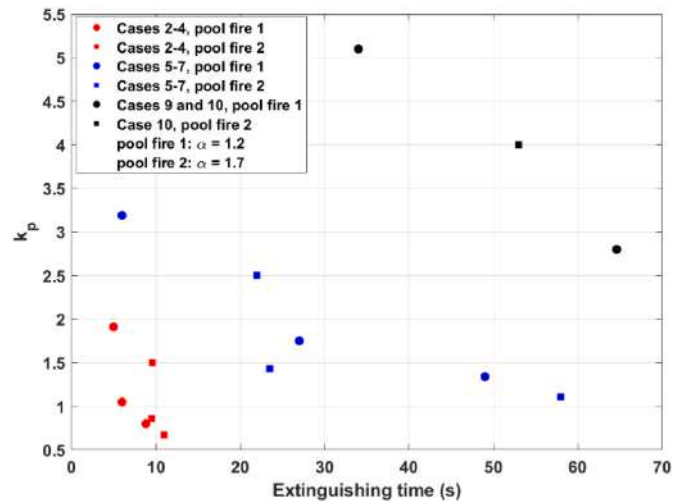


Fig. 16. Block ratio vs. suppression time.

Table 7
Characteristics and geometric parameters of all cases.

Case No.	Obstacle size (cm × cm)	Obstacle distance from the floor (cm)	L_o (m)	h_s (m)	h (m)	θ_0 (°)	L_f (m)	Extinguishing time (s)	Block ratio
1	0	0	–	–	2.23	–	0.25	4	0
2	15 × 15	60	0.15	1.73	2.23	4.96	0.25	4.5	0
							0.3	8.8	0.80
3	15 × 15	100	0.15	1.33	2.23	6.45	0.25	6	1.05
							0.3	9.5	0.87
4	15 × 15	160	0.15	0.73	2.23	11.73	0.25	5	1.91
							0.3	9.6	1.59
5	25 × 25	60	0.25	1.73	2.23	8.26	0.25	49	1.34
							0.3	58	1.12
6	25 × 25	100	0.25	1.33	2.23	10.74	0.25	27	1.75
							0.3	23.5	1.45
7	25 × 25	160	0.25	0.73	2.23	19.43	0.25	6	3.19
							0.3	22	2.65
8	40 × 40	60	0.4	1.73	2.23	13.19	0.25	Failed	2.15
							0.3	Failed	1.79
9	40 × 40	100	0.4	1.33	2.23	17.10	0.25	Failed	2.80
							0.3	Failed	2.33
10	40 × 40	160	0.4	0.73	2.23	30.64	0.25	34	5.10
							0.3	53	4.25

shielded fire applications is recommended by the authors for future works. Moreover, the possibility of using additives in water mist systems for extinguishing shielded fire scenarios will be studied.

CRedit authorship contribution statement

Azad Hamzehpour: Writing – review & editing, Writing – original draft, Visualization, Software, Resources, Project administration, Methodology, Investigation, Formal analysis, Data curation, Conceptualization. **Vittorio Verda:** Writing – review & editing, Supervision, Project administration, Methodology, Funding acquisition, Conceptualization. **Romano Borchiellini:** Writing – review & editing, Supervision, Project administration, Funding acquisition, Conceptualization.

Appendix

M1 – M12 temperatures for cases 1–10 for both pool pans are displayed here. It should be noted that only a few of the error bars are indicated in the plots for better visual purposes.

Declaration of competing interest

The authors declare that they have no known competing financial interests or personal relationships that could have appeared to influence the work reported in this paper.

Data availability

Data will be made available on request.

Acknowledgment

The authors wish to thank Mr. Maurizio Bressan for his technical assistance and consistent support in setting up the laboratory and carrying out the experiments.

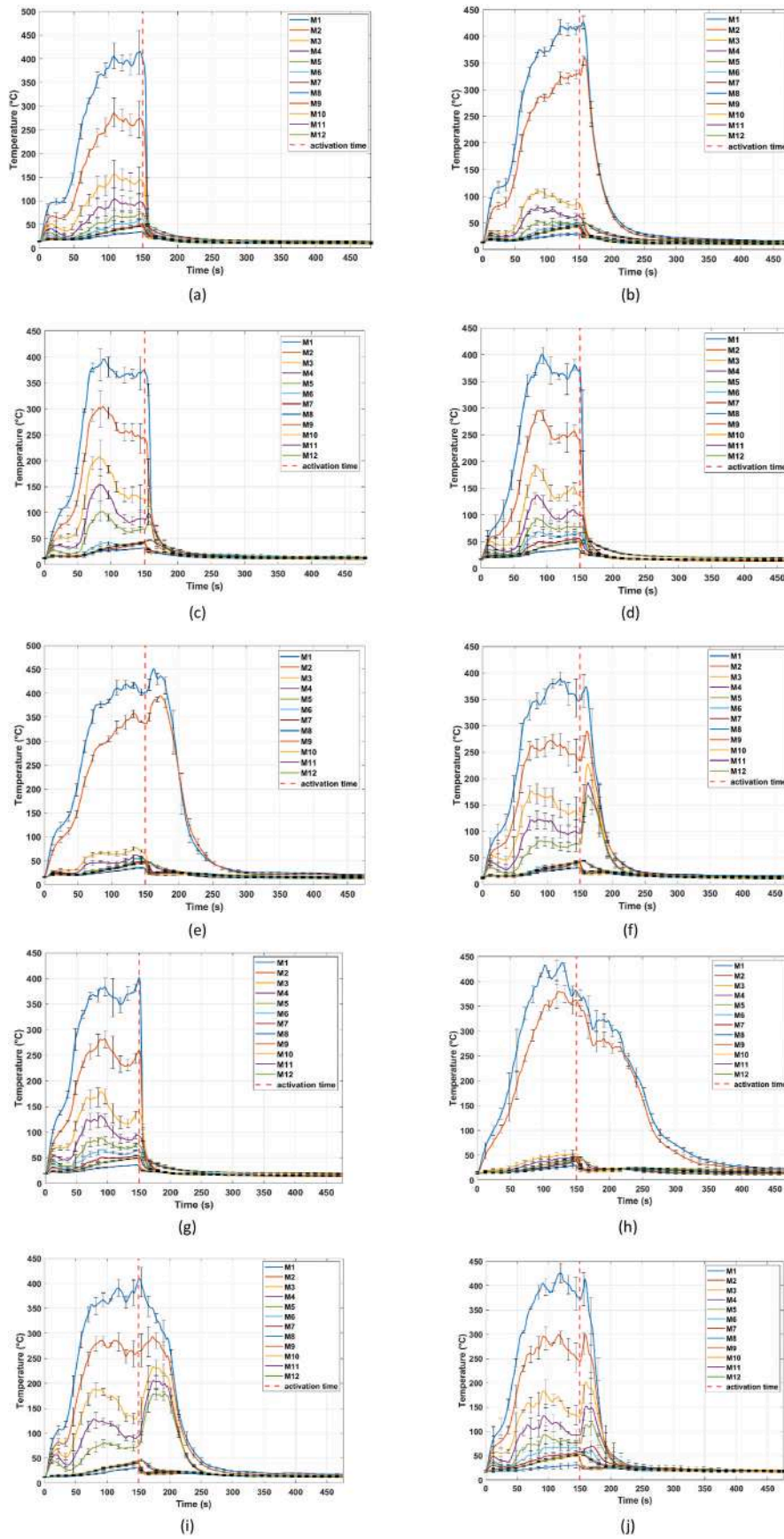


Fig. 17. M1 – M12 temperatures using pool pan 1 for: (a) case 1, (b) case 2, (c) case 3, (d) case 4, (e) case 5, (f) case 6, (g) case 7, (h) case 8, (i) case 9, (j) case 10

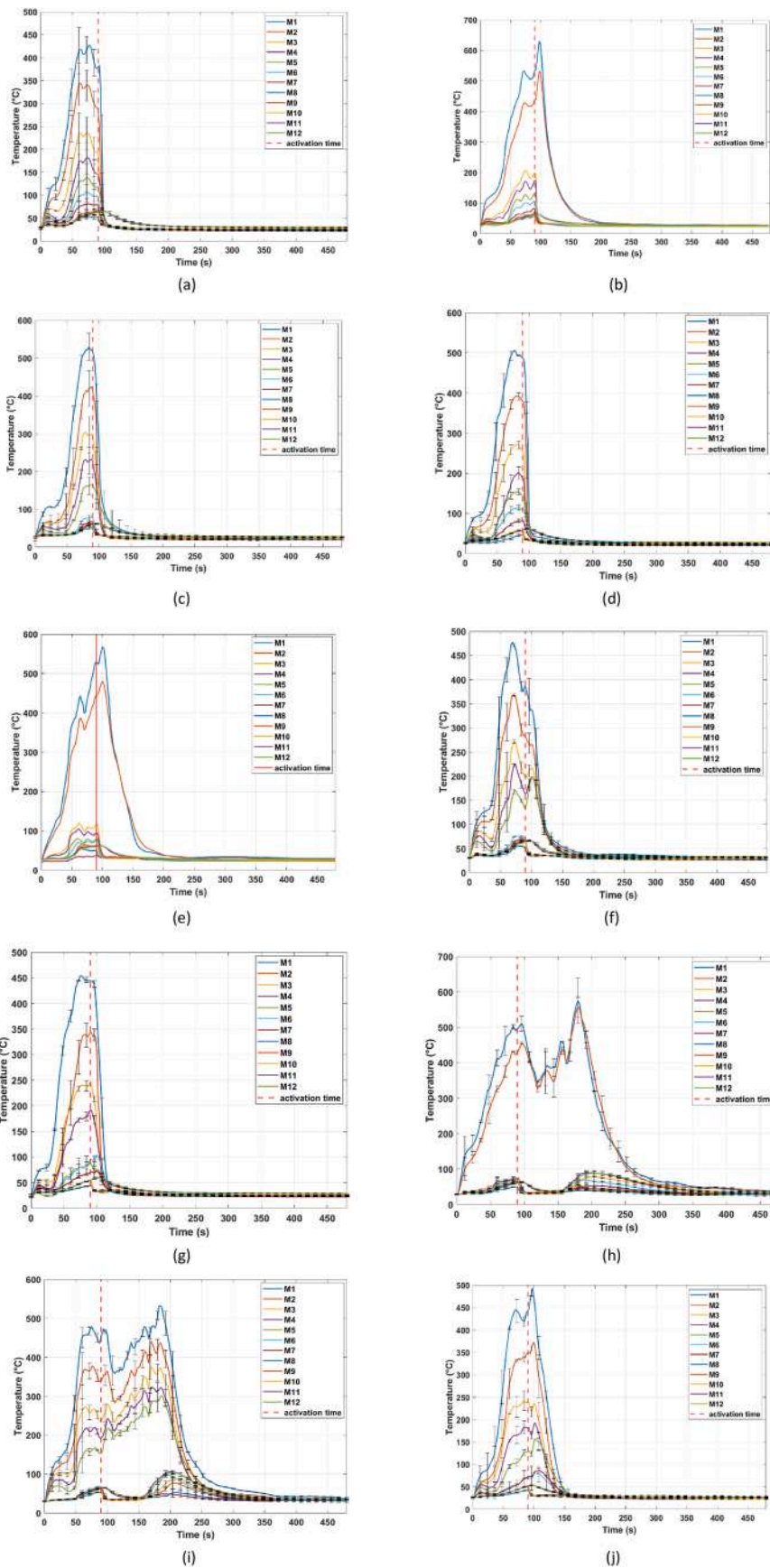


Fig. 18. M1 – M12 temperatures using pool pan 2 for: (a) case 1, (b) case 2, (c) case 3, (d) case 4, (e) case 5, (f) case 6, (g) case 7, (h) case 8, (i) case 9, (j) case 10

References

- [1] N.F.P. Association, NFPA 750-Standard on Water Mist Fire Protection Systems, 2006.
- [2] K. Farrell, M.K. Hassan, M.D. Hossain, B. Ahmed, P. Rahnamayiezekavat, G. Douglas, S. Saha, Water mist fire suppression systems for building and Industrial applications: Issues and Challenges, *Fire* (2023) 6, <https://doi.org/10.3390/fire620040>.
- [3] B. Yao, B.H. Cong, J. Qin, W.K. Chow, Experimental study of suppressing Poly (methyl methacrylate) fires using water mists, *Fire Saf. J.* 47 (2012) 32–39, <https://doi.org/10.1016/j.firesaf.2011.08.004>.
- [4] A. Jenft, A. Collin, P. Boulet, G. Pianet, A. Breton, A. Muller, Experimental and numerical study of pool fire suppression using water mist, *Fire Saf. J.* 67 (2014) 1–12, <https://doi.org/10.1016/j.firesaf.2014.05.003>.
- [5] M. Gupta, R. Rajora, S. Sahai, R. Shankar, A. Ray, S.R. Kale, Experimental evaluation of fire suppression characteristics of twin fluid water mist system, *Fire Saf. J.* 54 (2012) 130–142, <https://doi.org/10.1016/j.firesaf.2012.08.007>.
- [6] L. Yinshui, J. Zhuo, W. Dan, L. Xiaohui, Experimental research on the water mist fire suppression performance in an enclosed space by changing the characteristics of nozzles, *Exp. Therm. Fluid Sci.* 52 (2014) 174–181, <https://doi.org/10.1016/j.expthermflusci.2013.09.008>.
- [7] Z. Liu, A.K. Kim, J.Z. Su, Examination of performance of water mist fire suppression systems under ventilation conditions, *J. Fire Prot. Eng.* 11 (2001) 164–193.
- [8] Z. Liu, D. Carpenter, A.K. Kim, Characteristics of large cooking oil pool fires and their extinguishment by water mist, *J. Loss Prev. Process. Ind.* 19 (2006) 516–526, <https://doi.org/10.1016/j.jlp.2005.12.009>.
- [9] P. Zhang, X. Tang, X. Tian, C. Liu, M. Zhong, Experimental study on the interaction between fire and water mist in long and narrow spaces, *Appl. Therm. Eng.* 94 (2016) 706–714, <https://doi.org/10.1016/j.applthermaleng.2015.10.110>.
- [10] Y. Zhou, R. Bu, X. Zhang, C. Fan, J. Gong, Performance evaluation of water mist fire suppression: a clean and sustainable fire-fighting technique in mechanically-ventilated place, *J. Clean. Prod.* 209 (2019) 1319–1331, <https://doi.org/10.1016/j.jclepro.2018.10.315>.
- [11] L. Chen, W. Zhu, X. Cai, L. Pan, G. Liao, Experimental study of water mist fire suppression in tunnels under longitudinal ventilation, *Build. Environ.* 44 (2009) 446–455, <https://doi.org/10.1016/j.buildenv.2008.04.005>.
- [12] C. Fan, R. Bu, X. Xie, Y. Zhou, Full-scale experimental study on water mist fire suppression in a railway tunnel rescue station: temperature distribution characteristics, *Process Saf. Environ. Prot.* 146 (2021) 396–411, <https://doi.org/10.1016/j.psep.2020.09.019>.
- [13] Y. Liu, Z. Fang, Z. Tang, T. Beji, B. Merci, The combined effect of a water mist system and longitudinal ventilation on the fire and smoke dynamics in a tunnel, *Fire Saf. J.* 122 (2021) 103351, <https://doi.org/10.1016/j.firesaf.2021.103351>.
- [14] M. Gupta, A. Pasi, A. Ray, S.R. Kale, An experimental study of the effects of water mist characteristics on pool fire suppression, *Exp. Therm. Fluid Sci.* 44 (2013) 768–778, <https://doi.org/10.1016/j.expthermflusci.2012.09.020>.
- [15] Z. Wang, W. Wang, Q. Wang, Optimization of water mist droplet size by using CFD modeling for fire suppressions, *J. Loss Prev. Process. Ind.* 44 (2016) 626–632, <https://doi.org/10.1016/j.jlp.2016.04.010>.
- [16] Y.-M. Ferng, C.-H. Liu, Numerically investigating fire suppression mechanisms for the water mist with various droplet sizes through FDS code, *Nucl. Eng. Des.* 241 (2011) 3142–3148, <https://doi.org/10.1016/j.nucengdes.2011.06.002>.
- [17] A. Dasgotra, G. Rangarajan, S.M. Tauseef, CFD-based study and analysis on the effectiveness of water mist in interacting pool fire suppression, *Process Saf. Environ. Prot.* 152 (2021) 614–629, <https://doi.org/10.1016/j.psep.2021.06.033>.
- [18] T. Sikanen, J. Vaari, S. Hostikka, A. Paajanen, Modeling and simulation of high pressure water mist systems, *Fire Technol.* 50 (2014) 483–504, <https://doi.org/10.1007/s10694-013-0335-8>.
- [19] G.S. Settles, *Schlieren and Shadowgraph Techniques: Visualizing Phenomena in Transparent Media*, Springer Science & Business Media, 2001.
- [20] X. Wang, P. Zhu, Y. Li, X. Ni, M. Fan, Effect of low ambient air pressure on spray characteristics of water mist, *Exp. Therm. Fluid Sci.* 66 (2015) 7–12, <https://doi.org/10.1016/j.expthermflusci.2015.03.009>.
- [21] C.S. Jeong, C.Y. Lee, Experimental investigation on spray characteristics of twin-fluid nozzle for water mist and its heptane pool fire extinguishing performance, *Process Saf. Environ. Prot.* 148 (2021) 724–736, <https://doi.org/10.1016/j.psep.2021.01.037>.
- [22] P.E. Santangelo, Characterization of high-pressure water-mist sprays: experimental analysis of droplet size and dispersion, *Exp. Therm. Fluid Sci.* 34 (2010) 1353–1366, <https://doi.org/10.1016/j.expthermflusci.2010.06.008>.
- [23] H. Shrigondekar, A. Chowdhury, S.V. Prabhu, Characterization of a simplex water mist nozzle and its performance in extinguishing liquid pool fire, *Exp. Therm. Fluid Sci.* 93 (2018) 441–455, <https://doi.org/10.1016/j.expthermflusci.2018.01.015>.
- [24] B.P. Husted, P. Petersson, I. Lund, G. Holmstedt, Comparison of PIV and PDA droplet velocity measurement techniques on two high-pressure water mist nozzles, *Fire Saf. J.* 44 (2009) 1030–1045, <https://doi.org/10.1016/j.firesaf.2009.07.003>.
- [25] X. Wang, X. Wu, G. Liao, Y. Wei, J. Qin, Characterization of a water mist based on digital particle images, *Exp. Fluids.* 33 (2002) 587–593, <https://doi.org/10.1007/s00348-002-0509-5>.
- [26] G. Tian, H. Li, H. Xu, Y. Li, S.M. Raj, Spray characteristics study of DMF using phase Doppler particle analyzer, *SAE Int. J. Passeng. Cars-Mechanical Syst.* 3 (2010) 948–958.
- [27] B. Ditch, H.-Z. Yu, Characterization of water mist sprays using a phase-Doppler-Particle-Analyzer and an Iso-Kinetic Sampling probe, in: *ASME 2004 Heat Transf. Eng. Summer Conf.*, 2004, pp. 221–230, <https://doi.org/10.1115/ht-fed2004-56893>.
- [28] Y. Liu, X. Wang, T. Liu, J. Ma, G. Li, Z. Zhao, Preliminary study on extinguishing shielded fire with water mist, *Process Saf. Environ. Prot.* 141 (2020) 344–354, <https://doi.org/10.1016/j.psep.2020.05.043>.
- [29] C. Beihua, L. Guangxuan, H. Zhen, Extinction Limit of diesel pool fires suppressed by water mist, *J. Fire Sci.* 27 (2009) 5–26, <https://doi.org/10.1177/0734904108095337>.
- [30] R.L. Alpert, Numerical modeling of the interaction between automatic sprinkler sprays and fire plumes, *Fire Saf. J.* 9 (1985) 157–163, [https://doi.org/10.1016/0379-7112\(85\)90003-7](https://doi.org/10.1016/0379-7112(85)90003-7).
- [31] R. Bu, C. Fan, Z. Guo, Y. Zhou, Energy distribution analysis on suppressing a shielded fire with water mist in a tunnel rescue station, *Process Saf. Environ. Prot.* 158 (2022) 409–417, <https://doi.org/10.1016/j.psep.2021.12.022>.
- [32] A. Hamzehpour, V. Verda, R. Borchiellini, Simulation study on suppressing shielded fires by water mist systems, *Fire* 6 (2023), <https://doi.org/10.3390/fire6040129>.
- [33] C.-W. Chiu, Y.-H. Li, Full-scale experimental and numerical analysis of water mist system for sheltered fire sources in wind generator compartment, *Process Saf. Environ. Prot.* 98 (2015) 40–49, <https://doi.org/10.1016/j.psep.2015.05.011>.
- [34] H.-E. Albrecht, N. Damaschke, M. Borys, C. Tropea, *Laser Doppler and Phase Doppler Measurement Techniques*, Springer Science & Business Media, 2013.
- [35] H. Liu, M.C. Altan, Science and engineering of droplets: fundamentals and applications, *Appl. Mech. Rev.* 55 (2002) B16–B17.
- [36] V. Babrauskas, *Ignition Handbook: Principles and Applications to Fire Safety Engineering*, Fire Investigation, Risk Management and Forensic Science, Fire science publishers, 2003.
- [37] J. Wang, X. Cui, R. Zhang, Q. Xie, S. Zhang, L. Shi, Study on the mass loss rate of liquid pool fire in a well-confined ship cabin, *Int. J. Therm. Sci.* 166 (2021) 106984, <https://doi.org/10.1016/j.ijthermalsci.2021.106984>.
- [38] D. Sahu, S. Kumar, S. Jain, A. Gupta, Experimental and numerical simulation studies on diesel pool fire, *Fire Mater.* 40 (2016) 1016–1035, <https://doi.org/10.1002/fam.2361>.
- [39] C.C. Ndubizu, R. Ananth, P.A. Tatem, The effects of droplet size and injection Orientation on water mist suppression of low and high Boiling point liquid pool fires, *Combust. Sci. Technol.* 157 (2000) 63–86, <https://doi.org/10.1080/00102200008947310>.
- [40] Z. Liu, A.K. Kim, D. Carpenter, J.M. Kanabus-Kaminska, P.-L. Yen, Extinguishment of cooking oil fires by water mist fire suppression systems, *Fire Technol.* 40 (2004) 309–333, <https://doi.org/10.1023/B:FIRE.0000039161.18616.86>.
- [41] B. Downie, C. Polymeropoulos, G. Gogos, Interaction of a water mist with a buoyant methane diffusion flame, *Fire Saf. J.* 24 (1995) 359–381, [https://doi.org/10.1016/0379-7112\(95\)00029-1](https://doi.org/10.1016/0379-7112(95)00029-1).
- [42] P.E. Santangelo, B.C. Jacobs, N. Ren, J.A. Sheffel, M.L. Corn, A.W. Marshall, Suppression effectiveness of water-mist sprays on accelerated wood-crib fires, *Fire Saf. J.* 70 (2014) 98–111, <https://doi.org/10.1016/j.firesaf.2014.08.012>.
- [43] D. Drysdale, *An Introduction to Fire Dynamics*, John Wiley & Sons, 2011.
- [44] G. Heskestad, Virtual origins of fire plumes, *Fire Saf. J.* 5 (1983) 109–114, [https://doi.org/10.1016/0379-7112\(83\)90003-6](https://doi.org/10.1016/0379-7112(83)90003-6).
- [45] G. Heskestad, Engineering relations for fire plumes, *Fire Saf. J.* 7 (1984) 25–32, [https://doi.org/10.1016/0379-7112\(84\)90005-5](https://doi.org/10.1016/0379-7112(84)90005-5).